indicated a Cl···Cl contact of 1.7 Å, which was clearly not feasible.

Several precession photographs were taken of a second sample and examined carefully for doubling of one of the axes. Since there was no evidence for doubling, a large (0.45 × 0.55 × 0.70 mm) crystal was aligned on the goniostat and examined carefully for doubling of the axes, again with no success.

An examination of the final refinement indicated that the thermal parameters of Mo and Cl atoms not lying on the fourfold axis were larger by a factor of ca. 4 than those on the fourfold axis. This, and an examination of a Patterson synthesis, suggested the disorder, which was finally resolved. Mo(2) and Cl(4) were refined to 0.51 and 0.54 relative occupancies, with $R(F)$ dropping to 0.10. The occupancies were fixed at 0.50 for the remainder of the refinement.

Acknowledgment. We thank the National Science Foundation and the Wrubel Computing Center for support. D.L.C. was the 1983–1985 Indiana University SOHIO Graduate Fellow.

Registry No. I, 113794-50-6; II, 113794-55-1; III, 80878-94-0; IV, 80878-95-1; $Mo_2F_2(O\text{-}i\text{-}Pr)_4(PMe_3)_2$, 113794-51-7; $Mo_4Cl_3(O\text{-}i\text{-}Pr)_9$, 113794-52-8; $Mo_4I_3(O\text{-}i\text{-}Pr)_9$, 113794-54-0; $Mo_4I_4(O\text{-}i\text{-}Pr)_8$, 113794-53-9; $Mo_4O_2I_2(O\text{-}i\text{-}Pr)_6$, 113810-70-1; $Mo_4O_2Br_2(O\text{-}i\text{-}Pr)_6$, 113810-71-2; $Mo_2(O\text{-}i\text{-}Pr)_6$, 62521-20-4; PF_3, 7783-55-3; acetyl fluoride, 557-99-3; acetyl chloride, 75-36-5; chlorotrimethylsilane, 75-77-4; acetyl bromide, 506-96-7; bromotrimethylsilane, 2857-97-8; iodotrimethylsilane, 16029-98-4.

Supplementary Material Available: Listings of anisotropic thermal parameters, complete listings of bond distances and bond angles, and selected stereoviews for the molecules $Mo_4Br_4(O\text{-}i\text{-}Pr)_8$, $Mo_4Cl_4(O\text{-}i\text{-}Pr)_8$, $Mo_4Br_3(O\text{-}i\text{-}Pr)_9$, and $Mo_4F_2(O\text{-}i\text{-}Pr)_{10}$ (22 pages); listings of F_o and F_c values for the four compounds (63 pages). Ordering information is given on any current masthead page.

Contribution from the Departments of Chemistry, The Ohio State University, Columbus, Ohio 43210, and Indiana University, Bloomington, Indiana 47405

Electronic Structure and Bonding in Halide- and Alkoxide-Supported Tetranuclear Molybdenum Clusters

B. E. Bursten,*† M. H. Chisholm,*‡ and D. L. Clark‡

Received September 30, 1987

The bonding within square, rectangular, and butterfly tetranuclear molybdenum clusters, Mo_4^{12+}, supported in varying degrees by μ_3-X, μ_2-X, and terminal X ligands (X = Cl^-, OH^-) has been examined by nonempirical Fenske–Hall molecular orbital calculations. Mulliken populations of the canonical valence orbitals of the cluster framework are shown to vary with different ligand environments, which allows for the metal–metal bonding to be traced through successive stages of ligation. The calculations indicate that both capping and edge-bridging ligands cause the movement of charge out of the main metal–metal cluster-bonding orbitals, resulting in occupation of higher lying metal–metal nonbonding and antibonding orbitals. The bonding in the butterfly clusters $Mo_4(\mu_3\text{-}X)_2(\mu_2\text{-}X)_4X_6$ (X = OH^-, Cl^-) is shown to be dominated by the influence of the capping ligands whereas the square clusters of formula $Mo_4(\mu_2\text{-}X)_8X_4$ are shown to be dominated by edge-bridging ligands. Radial ligands on both the square and butterfly clusters are shown to be in competition for σ-density between metal–metal cluster bonding and radial metal–ligand bonding, and this phenomenon has been termed the *radial cluster influence*. It is shown that the rectangular cluster $Mo_4(\mu_2\text{-}Cl)_8Cl_4^{3-}$ is closely related to the square cluster of the same general formula, and the rectangular geometry can be understood as a result of a first-order Jahn–Teller distortion of the regular D_{4h} square structure in analogy with the case for the cyclobutadiene radical cation.

Introduction

Within the past several years a very rich and beautiful chemistry of halide- and alkoxide-supported tetranuclear molybdenum clusters has begun to emerge. One fascinating aspect of this chemistry is the similarity in structural geometries for halide- and alkoxide-supported clusters. Compounds of formula $Mo_4X_4(O\text{-}i\text{-}Pr)_8$ exhibit square and butterfly geometries in the solid state for X = Cl and Br, respectively, although the butterfly geometry is the dominant species in solution.[1,2] Similarly, the new chloromolybdate ions of formula $Mo_4Cl_{12}^{3-}$ display rectangular and butterfly geometries depending on the nature of the counterion, while the rectangular geometry seems to prevail in solution.[3] The iodomolybdate ion of formula $Mo_4I_{11}^{2-}$ also displays a butterfly geometry[4,5] closely related to that shared by $Mo_4Br_4(O\text{-}i\text{-}Pr)_8$ and $Mo_4Cl_{12}^{3-}$. The prototypical square and butterfly structures of general formula $Mo_4(\mu_2\text{-}X)_8X_4$ and $Mo_4(\mu_3\text{-}X)_2(\mu_2\text{-}X)_4X_6$ are shown in Figure 1. These general cluster types both contain Mo_4 units within a cube of X ligands and as such may be viewed as arachno derivatives of the well-known closo octahedral $Mo_6(\mu_3\text{-}X)_8X_6^{2-}$ cluster.[6-8] These cube–octahedral relationships are shown in I with the closo $Mo_6(\mu_3\text{-}X)_8^{4+}$ structure appearing in Ia. In the basic $Mo_6(\mu_3\text{-}X)_8^{4+}$ unit, the six molybdenum atoms define an octahedron, and the eight μ_3-X ligands symmetrically cap the triangular faces of the Mo_6 skeleton. The six metal atoms are also coordinated to six terminal ligands, which radiate from the vertices of the Mo_6 octahedron. By removal of two opposite

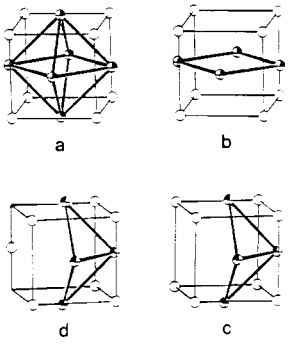

I

Mo vertices, one obtains the arachno Mo_4 square derivative shown in Ib, which yields eight doubly bridging X ligands while the terminal ligands radiate from the Mo vertices. In a similar fashion,

† The Ohio State University.
‡ Indiana University.

(1) Chisholm, M. H.; Errington, R. J.; Folting, K.; Huffman, J. C. *J. Am. Chem. Soc.* **1982**, *104*, 2025.
(2) Chisholm, M. H.; Clark, D. L.; Errington, R. J.; Folting, K.; Huffman, J. C. *Inorg. Chem.*, preceding article in this issue.
(3) Aufdembrink, B. A.; McCarley, R. E. *J. Am. Chem. Soc.* **1986**, *108*, 2474.
(4) Stensvad, S.; Helland, B. J.; Babich, M. W.; Jacobson, R. A.; McCarley, R. E. *J. Am. Chem. Soc.* **1978**, *100*, 6257.
(5) Glicksman, H. D.; Walton, R. A. *Inorg. Chem.* **1978**, *17*, 3197.
(6) Schafer, H.; von Schnering, H. G. *Angew. Chem.* **1971**, *385*, 75.
(7) Guggenberger, L. J.; Sleight, A. W. *Inorg. Chem.* **1969**, *8*, 2041.
(8) Healy, P. C.; Kepert, D. L.; Taylor, D.; White, A. W. *J. Chem. Soc., Dalton Trans.* **1973**, 646.

0020-1669/88/1327-2084$01.50/0

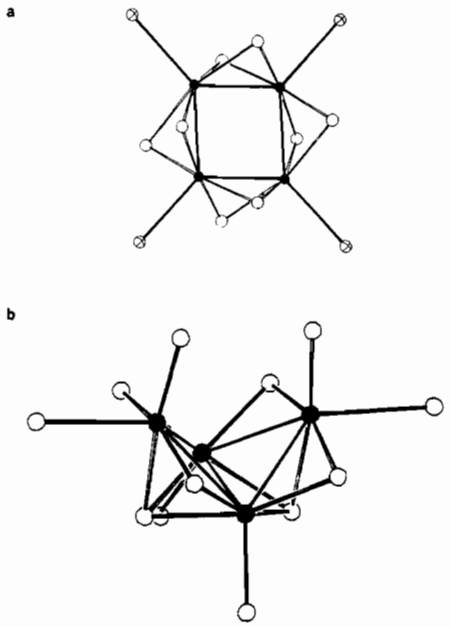

Figure 1. Central structural unit of tetranuclear molybdenum clusters: (a) square structure of general formula $Mo_4(\mu_2\text{-}X)_8X_4$; (b) butterfly structure of general formula $Mo_4(\mu_3\text{-}X)_2(\mu_2\text{-}X)_4X_6$. Metal positions are indicated by filled circles; X ligands are indicated by open circles.

removal of two adjacent vertices yields the Mo_4 butterfly structure shown in Ic and represents an alternate arachno derivative of the Mo_6 octahedron. This gives rise to two triply bridging, four doubly bridging, and six terminal ligands, four of which radiate from the Mo vertices. The butterfly structure is closely related to the $Mo_4I_{11}^{2-}$ structure reported by McCarley et al.[4] The latter also contains a butterfly Mo_4 core and may also be viewed as a derivative of the Mo_6 octahedron. The central $Mo_4I_7^{2+}$ core contains six I^- ligands at the corners of the cube, while the seventh bridges the two wingtip atoms at the midpoint of the edge of the idealized I_8 cube as shown in Id.

A fundamental knowledge about the electronic structures of such clusters may provide a basis for understanding the bonding and reactivity properties of these new materials and perhaps even the ability to predict new structures. For example, accurate knowledge about the electronic structures of aromatic organic compounds has led to detailed theories for their thermal and photochemical activity.[9,10] By comparison, the electronic structures of transition-metal compounds are much less well-defined, due in part to their greater complexity.

There exists a variety of approaches toward understanding the bonding in the closely related halide- and alkoxide-supported clusters. The octahedral $Mo_6(\mu_3\text{-}X)_8X_6^{2-}$ cluster has been the subject of numerous calculational studies ranging in methodology from the d-orbital overlap model of Cotton and Haas to the Xα–SW formalism.[7,11-14] Very recently, much interest has been focused on the role of π-acceptor versus π-donor ligands on the Mo_6 cluster core,[15-17] and the nido and arachno derivatives have been interpreted within the framework of Stone's tensor surface harmonic theory.[17] Another approach toward understanding the bonding in these tetranuclear clusters could be to view the molecular orbitals of the Mo_4 framework in the context of combining four ML_5 octahedral fragments.[18] This method is quite satisfactory toward gaining a qualitative understanding of metal–metal bonding within the Mo_4 framework yet provides little information concerning the electronic influence of the ligands. Therefore, in order to facilitate a separation of metal–metal and metal–ligand bonding, we present here an alternative "clusters-in-molecules" approach, which has proven successful in understanding the bonding in related trinuclear[19,20] and tetranuclear[21] metal atom clusters. This approach emphasizes how the interactions of the valence orbitals of the cluster framework vary with different ligand environments. In this fashion, the bonding characteristics of the Mo_4 cluster as a central entity surrounded by ligands are kept at the center of attention. We have employed the Fenske–Hall molecular orbital method[22] to obtain numerical results for the tetranuclear clusters. To implement the "clusters-in-molecules" formalism, it is useful first to discuss the bonding in the "naked" Mo_4^{12+} cluster core. Due to its high symmetry, we begin our discussion with the D_{4h} square cluster core.

Results and Discussion

(1) Halide- and Alkoxide-Supported Square and Rectangular Mo_4 Clusters. The D_{4h} Mo_4^{12+} Core. In our discussion of the D_{4h} Mo_4^{12+} cluster core, it is convenient to employ a right-handed local coordinate system on each metal atom in which the z axis points toward the center of the square, the x axis is in the plane of the square, and the y axis is perpendicular to the plane. This coordinate system is shown in II. Under D_{4h} symmetry, the Mo

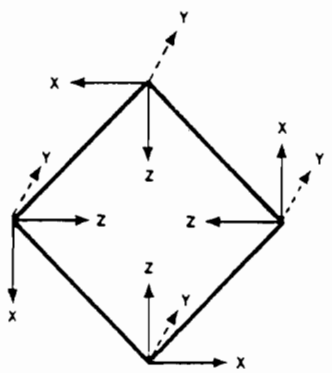

II

4d atomic orbitals in this coordinate system are transformed as the irreducible representations

$$z^2\text{: } a_{1g} + b_{1g} + e_u$$

$$x^2 - y^2\text{: } a_{1g} + b_{1g} + e_u$$

$$xz\text{: } a_{2g} + b_{2g} + e_u$$

$$yz\text{: } a_{2u} + b_{2u} + e_g$$

$$xy\text{: } a_{1u} + b_{1u} + e_g$$

The relative energies and Mulliken percent characters of the primarily 4d molecular orbitals of Mo_4^{12+} are given in Table I. From the table it is clear that our choice of local coordinates results in molecular orbitals that retain, to a large extent, the character of only one type of atomic orbital, even when mixing is allowed by symmetry. The 12 valence electrons are expected to occupy the $1a_{1g}$, $1a_{2u}$, $1b_{2g}$, $1b_{1u}$, $2a_{1g}$, and $1e_u$ levels, which are depicted qualitatively in III. The $1e_u$ orbital, which is only doubly occupied, is the HOMO of the cluster. The $1a_{1g}$ and $2a_{1g}$ orbitals may be regarded as the σ-bonding combinations of the Mo $4d_{z^2}$ and $4d_{x^2-y^2}$

(9) Woodward, R. B.; Hoffmann, R. *The Conservation of Orbital Symmetry*; Academic: New York, 1969.
(10) Salem, L. *Electrons in Chemical Reactions*; Wiley: New York, 1982.
(11) Cotton, F. A.; Haas, T. E. *Inorg. Chem.* **1964**, *3*, 10.
(12) Cotton, F. A.; Stanley, G. G. *Chem. Phys. Lett.* **1979**, *58*, 450.
(13) Bursten, B. E.; Cotton, F. A.; Stanley, G. G. *Isr. J. Chem.* **1980**, *19*, 132.
(14) Seifert, G.; Grossmann, G.; Muller, H. *J. Mol. Struct.* **1980**, *64*, 93.
(15) Woolley, R. G. *Inorg. Chem.* **1985**, *24*, 3519.
(16) Woolley, R. G. *Inorg. Chem.* **1985**, *24*, 3525.
(17) Johnston, R. J.; Mingos, D. M. P. *Inorg. Chem.* **1986**, *25*, 1661.
(18) Elian, M.; Hoffmann, R. Inorg. *Chem.* **1975**, *14*, 1058.
(19) Bursten, B. E.; Cotton, F. A.; Hall, M. B.; Najjar, R. C. *Inorg. Chem.* **1982**, *21*, 302.
(20) Chisholm, M. H.; Cotton, F. A.; Fang, A.; Kober, E. M. *Inorg. Chem.* **1984**, *23*, 749.
(21) Cotton, F. A.; Fang, A. *J. Am. Chem. Soc.* **1982**, *104*, 113.
(22) Hall, M. B.; Fenske, R. F. *Inorg. Chem.* **1972**, *11*, 768.

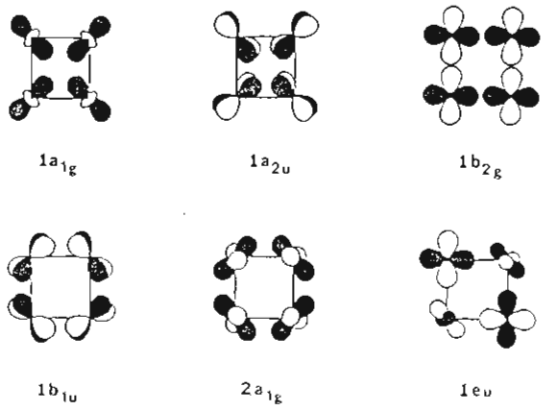

III

AO's, respectively, although it is seen in Table I that the sets of these two AO's are slightly mixed in Mo_4^{12+}, a result that will have important consequences when ligands are introduced into the bonding picture. The $1a_{2u}$ and $1b_{1u}$ orbitals may be regarded as π-bonding combinations of the Mo $4d_{yz}$ and $4d_{xy}$ AO's respectively. The $1b_{2g}$ orbital is the σ-bonding combination of Mo $4d_{xz}$ AO's, and finally, the $1e_u$ orbital is a mixture of primarily Mo $4d_{xz}$ with some Mo $4d_{x^2-y^2}$ contribution. One of the pair of $1e_u$ orbitals is shown qualitatively in III.

Bridging Ligands. The question of how edge-bridging ligands bond to the D_{4h} Mo_4^{12+} cluster framework will be addressed first by investigating the electronic structure of the D_{4h} core, $Mo_4(\mu_2\text{-}X)_8^{4+}$, where X = Cl^- or OH^-. Neglect of the radial or terminally bonded ligands allows us to focus upon the influence of bridging ligands only, without having to sort out the effects due to the radial ligands.

A correlation diagram that traces the perturbations imposed by the bridging ligands on the canonical orbitals of Mo_4^{12+} is shown in Figure 2. We note that almost all of the canonical orbitals of Mo_4^{12+} are destabilized by interaction with the bridging ligands. For each symmetry type, some metal–metal bonding is sacrificed to facilitate metal–ligand bonding. The magnitude of the destabilization can be taken as a rough measure of the stabilizing interaction occurring in lower lying metal–ligand bonding orbitals. A major portion of the metal–ligand bonding occurs via donation from the bridging ligand orbitals into empty nonbonding and antibonding orbitals of Mo_4^{12+}. Figure 2 illustrates the difference between the $(\mu_2\text{-}Cl)_8^{8-}$ and $(\mu_2\text{-}OH)_8^{8-}$ ligand sets. Qualitatively, the O 2p orbitals lie below the "d block" of Mo_4^{12+} cluster orbitals, and as expected from simple perturbation theory, interaction pushes the metal–metal bonding levels up in energy such that in $Mo_4(\mu_2\text{-}OH)_8^{4+}$ there is essentially a block of cluster Mo–Mo framework-bonding orbitals at higher energy, a block of O 2p lone-pair orbitals at intermediate energy, and Mo–O σ-bonding orbitals at lower energy. Conversely, for $Mo_4(\mu_2\text{-}Cl)_8^{4+}$ we find that the Cl 3p atomic orbitals lie slightly above the "d block", more metal–ligand mixing is observed, and Cl 3p lone-pair orbitals end up becoming the two highest occupied molecular orbitals. For $Mo_4(\mu_2\text{-}Cl)_8^{4+}$ the destabilization of the Mo_4^{12+} cluster framework-bonding orbitals is less than that observed for $Mo_4(\mu_2\text{-}OH)_8^{4+}$ and the $1b_{2g}$ metal–metal σ-bonding level is actually stabilized by the interaction. We attribute this to the energetic difference between O 2p and Cl 3p atomic orbitals relative to the Mo 4d atomic orbitals as well as the greater Mo–O overlap and from this deduce that the $(\mu_2\text{-}OH)_8^{8-}$ ligand set has a greater destabilizing influence on the Mo_4^{12+} core orbitals than the $(\mu_2\text{-}Cl)_8^{8-}$ ligand set.

Let us now examine the behavior of the $1a_{2u}$, $1a_{2g}$, $1b_{2g}$, $1b_{1u}$, $2a_{1g}$, and $1e_u$ metal–metal bonding orbitals of Mo_4^{12+}, which were occupied in the "naked" Mo_4^{12+} cluster. The $1b_{1u}$ orbital of Mo_4^{12+} is directed to the site of the incoming bridging ligands and is removed from the frontier region by ligand σ-donation. The $1e_u$ orbital, which was only doubly occupied in Mo_4^{12+}, accommodates these two electrons in the $Mo_4(\mu_2\text{-}X)_8^{4+}$ fragments. These observations are amplified by the Mulliken populations of the

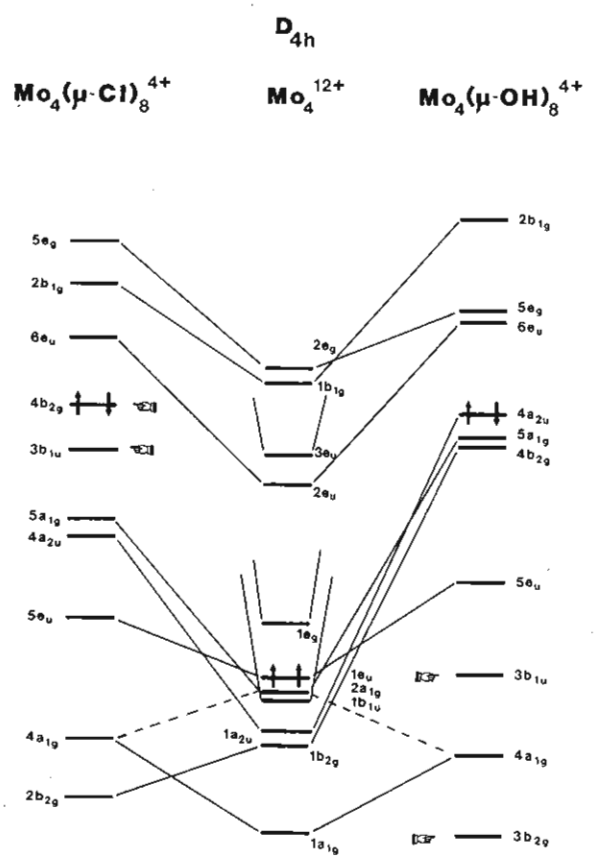

Figure 2. Correlation diagram comparing the effect of the $(\mu_2\text{-}X)_8^{8-}$ ligand set on the relative energies of the D_{4h} Mo_4^{12+} cluster orbitals. The HOMO's of each cluster fragment are denoted by arrows. Note: the $1e_u$ orbital of Mo_4^{12+} is only doubly occupied and as such represents a diradical. The b_{1u} and b_{2g} orbitals, denoted by hands, represent X (X = Cl^-, OH^-) lone-pair orbitals, and thus the HOMO of $Mo_4(\mu_2\text{-}Cl)_8^{4+}$ is a chlorine lone-pair orbital.

canonical orbitals of Mo_4^{12+} in the clusters $Mo_4(\mu_2\text{-}Cl)_8^{4+}$ and $Mo_4(\mu_2\text{-}OH)_8^{4+}$, given in Table II. From the table it can be seen that the presence of edge-bridging ligands results in the transfer of charge out of the $1b_{1u}$ orbital such that its Mulliken population is decreased to less than 1e. Very little charge is transferred out of the remaining occupied orbitals of Mo_4^{12+}; rather, the empty nonbonding orbitals $1e_g$, $2e_u$, $3e_u$, and $2e_g$ act as ligand acceptor orbitals. Although the net effect of edge-bridging ligands is a destabilization of the manifold of metal–metal cluster-bonding orbitals, the metal–metal bonding is preserved despite the introduction of metal–ligand bonding.

Radial Ligands. The influence of radial ligands on the Mo_4^{12+} core is much different from that of the bridging ligands just discussed. The set of Cl 3p σ lone-pair orbitals span $a_{1g} + b_{1g} + e_u$ symmetry, and the primary bonding interactions between the Mo_4^{12+} core and the radial chloride ligands are σ-donations into the empty $2b_{1g}$ (d_{z^2}) metal–metal antibonding and $2e_u$ (d_{xz}, $d_{x^2-y^2}$) nonbonding cluster orbitals, the latter of which appears as a pronounced increase in the Mulliken population of the $2e_u$ orbital of Mo_4^{12+} in $Mo_4Cl_4^{8+}$ shown in Table II. Most important is the radial ligand effect on the a_{1g} metal–metal σ-bonding orbitals. Recall that, in Mo_4^{12+}, the Mo $4d_{z^2}$ and $4d_{x^2-y^2}$ atomic orbitals were slightly mixed in the $1a_{1g}$ and $2a_{1g}$ molecular orbitals (Table I). The radial ligand a_{1g} σ-interaction forces a rehybridization of the metal-based a_{1g} orbitals in an attempt to preserve metal–metal σ-bonding. As a consequence, in $Mo_4Cl_4^{8+}$ the Cl 3p σ-character is spread out over three MO's of a_{1g} symmetry: one bonding, one nonbonding, and one antibonding. The lower lying bonding orbital is *both* Mo–Mo and Mo–Cl σ-bonding, and the higher lying orbitals are strongly hybridized. In essence, the a_{1g} σ-interaction transfers a portion of the $2a_{1g}$ orbital of Mo_4^{12+} into the unoccupied $4a_{1g}$ orbital of $Mo_4Cl_4^{8+}$, which allows for concomitant mixing of virtual Mo 5s and $5p_z$ character into the $3a_{1g}$

Table I. Relative Orbital Energies and Atomic Orbital Populations for the Primarily 4d Valence Molecular Orbitals of D_{4h} Mo_4^{12+}

orbital	rel E, eV	% contribn[a]						
		z^2	x^2-y^2	xy	xz	yz	s	p
$1a_{1g}$	−21.87	85	14				0	1
$1a_{2u}$	−18.99					99		1
$1b_{2g}$	−18.02				100			0
$1b_{1u}$	−17.79			100				
$2a_{1g}$	−17.33	12	80				8	0
$1e_u$	−16.42	1	19		71		9	0
$1e_g$	−15.32			62		37		1
$2e_u$	−10.95	31	54		10		0	5
$3e_u$	−10.24	56	26		5		10	3
$1b_{1g}$	−8.19	29	65				6	0
$2e_g$	−7.34			30		58		12
$1b_{2u}$	−5.99					91		9
$1a_{1u}$	−1.95			100				
$2b_{1g}$	−1.72	53	11				11	25
$1a_{2g}$	0.00				95			5

[a] Blank entries are zero by symmetry.

Table II. Mulliken Populations of the Canonical Orbitals of D_{4h} Mo_4^{12+} for $Mo_4Cl_4^{8+}$, $Mo_4(\mu\text{-}Cl)_8^{4+}$, $Mo_4(\mu\text{-}OH)_8^{4+}$, $Mo_4(\mu\text{-}Cl)_8Cl_4$, and $Mo_4(\mu\text{-}OH)_8Cl_4$ Clusters

orbital	Mo_4^{12+}	$Mo_4Cl_4^{8+}$	$Mo_4(\mu\text{-}Cl)_8^{4+}$	$Mo_4(\mu\text{-}OH)_8^{4+}$	$Mo_4(\mu\text{-}Cl)_8Cl_4$	$Mo_4(\mu\text{-}OH)_8Cl_4$
$1a_{1g}$	2.00	1.81	1.94	1.87	1.91	1.83
$1a_{2u}$	2.00	1.43	1.95	1.92	1.97	1.94
$1b_{2g}$	2.00	1.40	2.00	1.98	2.00	1.99
$1b_{1u}$	2.00	2.00	0.95	0.71	0.88	0.66
$2a_{1g}$	2.00	1.08	1.94	1.95	1.94	1.92
$1e_u$	2.00	3.72	3.78	3.58	3.82	3.66
$1e_g$	0.00	3.94	2.03	1.54	1.76	1.40
$2e_u$	0.00	1.58	0.90	0.92	1.20	1.04
$3e_u$	0.00	0.10	1.22	1.40	1.16	1.34
$1b_{1g}$	0.00	0.00	0.33	0.52	0.47	0.51
$2e_g$	0.00	0.92	1.10	1.04	0.74	0.66

and $4a_{1g}$ MO's, respectively. These effects are evident in the Mulliken populations of the canonical orbitals of Mo_4^{12+} in $Mo_4Cl_4^{8+}$ shown in Table II. It is seen that the interaction of the Mo_4^{12+} orbitals with the radial chloride ligands favors the transfer of charge out of the $1a_{2u}$, $1b_{2g}$, and $2a_{1g}$ metal–metal bonding orbitals of Mo_4^{12+} and that empty orbitals of e_g and e_u symmetry act as charge acceptors. The rehybridization of a_{1g} metal–metal σ-bonding orbitals and their resulting decrease in Mulliken population can be viewed as an attempt to preserve metal–metal σ-bonding at the expense of radial metal–ligand σ-bonding. We will refer to this competition for σ-density as the *radial cluster influence*. The importance of this in the cluster bonding is significantly altered when bridging ligands are present. For example, it will be shown that the transfer of charge out of the $1a_{2u}$ and $1b_{2g}$ orbitals of Mo_4^{12+}, which results from the π-interaction between the cluster core and the set of Cl 3p π-orbitals, is of little importance when the bridging ligands are present.

Ligand Preference. The above analysis shows a nice dichotomy in the mode of bonding of bridging and terminal ligands to the Mo_4^{12+} framework. The bridging ligands bind primarily via donation into the empty frontier orbitals of the metal framework. As a result, the Mo–Mo bonding present in the naked cluster is not severely affected. By contrast, the radial ligands were found to force a rehybridization of the a_{1g} metal–metal σ-bonding orbitals, resulting in mixing of Mo 4d and virtual 5s and $5p_z$ atomic orbitals and concomitant depopulation of some of the metal–metal bonding orbitals. Inspection of Table II shows that the changes induced by the two types of ligands are, to a large extent, mutually exclusive; i.e., many of the orbitals that are perturbed strongly by terminal ligands are relatively unperturbed by bridging ligands. We can use this to determine which ligands dominate the electronic structure of a cluster in which *both* bridging and terminal ligands are present, and in this section we will examine the bonding in the complete $Mo_4(\mu_2\text{-}X)_8Cl_4$ molecules ($X = Cl^-, OH^-$). Our MO calculations on these systems indicate that the bridging ligands influence the cluster core more than the radial ligands. This observation is demonstrated nicely by the Mulliken populations of Table II. From the table it can be seen that the Mulliken

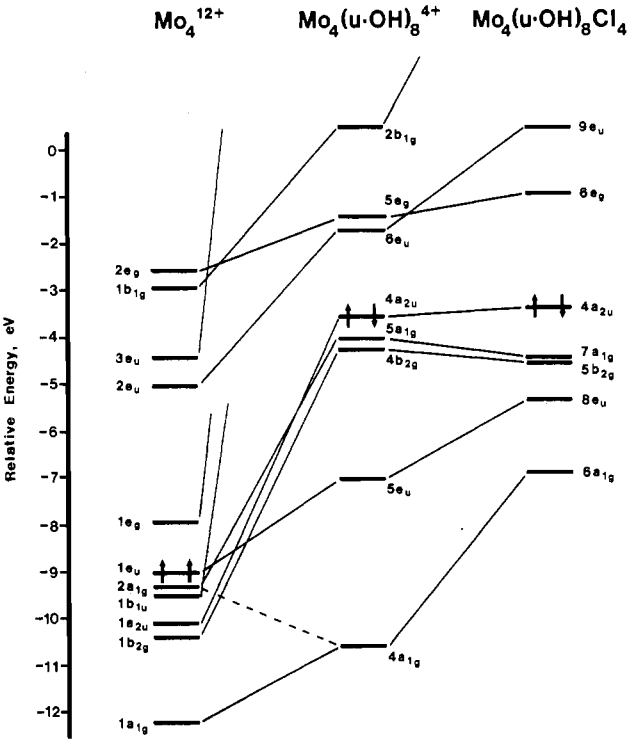

Figure 3. Correlation diagram tracing the perturbations of the primarily metal–metal bonding orbitals of D_{4h} Mo_4^{12+} (left) as ligation occurs through (1) introduction of eight μ-OH ligands (center) and (2) introduction of the four radial Cl ligands (right). The HOMO for each degree of perturbation is denoted by arrows. Note: the $1e_u$ orbital of Mo_4^{12+} is only doubly occupied and as such represents a diradical.

populations of the Mo_4^{12+} core orbitals in $Mo_4(\mu_2\text{-}Cl)_8Cl_4$ and $Mo_4(\mu_2\text{-}OH)_8Cl_4$ closely resemble those of $Mo_4(\mu_2\text{-}Cl)_8^{4+}$ and $Mo_4(\mu_2\text{-}OH)_8^{4+}$. Thus, the populations reflect the dominant influence of the bridging ligands on the Mo_4 framework-bonding

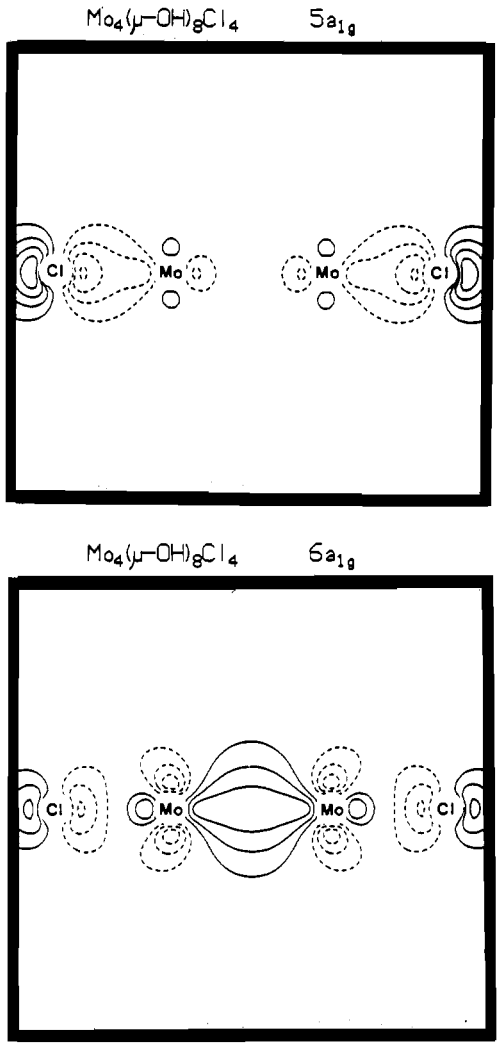

Figure 4. Contour plots comparing the occupied $5a_{1g}$ (top) and $6a_{1g}$ (bottom) orbitals of D_{4h} $Mo_4(\mu\text{-}OH)_8Cl_4$. Positive and negative contour values are represented by solid and dashed lines, respectively. Contour values for this and all subsequent plots begin at ± 0.02 e/Å^3 and increase by a factor of 2 at each step. These plots are taken as a slice across the diagonal of the square as one looks parallel to the edge of the Mo_4 plane.

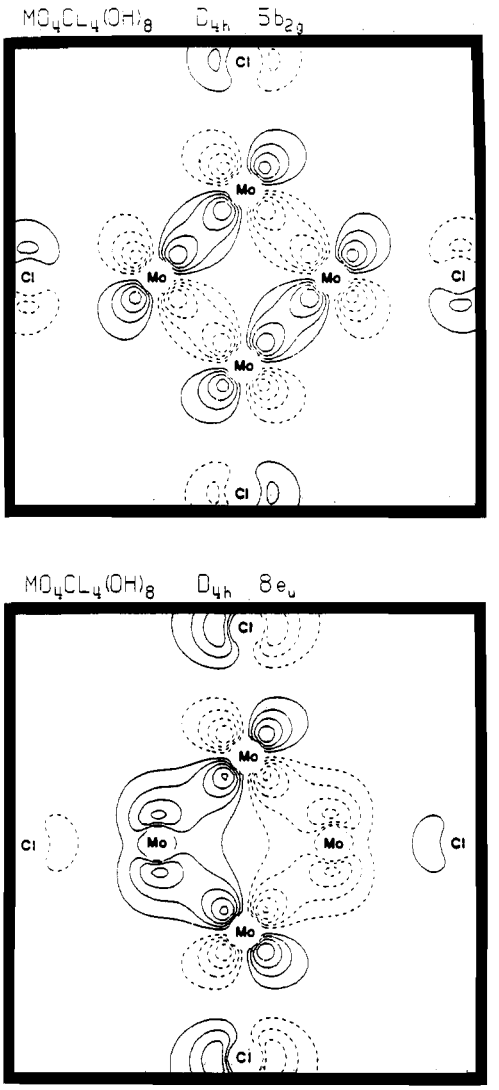

Figure 5. Contour plots of the occupied primarily metal–metal bonding $5b_{2g}$ (top) and $8e_u$ (bottom) orbitals of D_{4h} $Mo_4(\mu\text{-}OH)_8Cl_4$. These plots are in the Mo_4 plane containing the four Mo atoms and four radial Cl ligands.

orbitals, and none of the effects attributable to the radial ligands that were seen for $Mo_4Cl_4^{8+}$ are observed in the populations of the "complete" clusters. The effects of the ligand sets upon the orbitals of Mo_4^{12+} apparently follow the ordering

$$(\mu_2\text{-}OH)_8^{8-} > (\mu_2\text{-}Cl)_8^{8-} \gg Cl_4^{4-}$$

The perturbations of these ligand sets can be applied in sequence, and Figure 3 shows the correlation of the orbitals of Mo_4^{12+}, $Mo_4(\mu_2\text{-}OH)_8^{4+}$, and $Mo_4(\mu_2\text{-}OH)_8Cl_4$. This sequence is instructive in that it demonstrates not only that the bridging OH^- ligands are energetically the most important but also that their influence dominates the final ordering of occupied MO's. In the $Mo_4(\mu_2\text{-}OH)_8Cl_4$ cluster, the rehybridization of a_{1g} cluster-bonding orbitals induced by terminal chloride ligands is evident. However, the relative energies of these cluster a_{1g} orbitals have been "fixed" by the dominant influence of the bridging ligand. This has important ramifications toward Mo–Mo versus Mo–Cl σ-bonding when both bridging and terminal ligands are present. The lower lying $5a_{1g}$ orbital of $Mo_4(\mu_2\text{-}OH)_8Cl_4$ is predominantly the in-phase combination of Mo $4d_{z^2}$ and Cl $3p\sigma$ atomic orbitals and is Mo–Cl σ-bonding, while the higher lying $6a_{1g}$ orbital is Mo–Mo σ-bonding and Mo–Cl σ-antibonding. Thus, even in the presence of the dominant bridging ligands, rehybridization of a_{1g} cluster orbitals is induced by the radial σ-donors, although, since both levels are filled, little net Mo–Cl σ-bonding results. The rehybridization of the a_{1g} orbitals is evident in contour diagrams of the $5a_{1g}$ and $6a_{1g}$ orbitals, shown in Figure 4. These diagrams show a slice of the orbitals in a perpendicular bisector of a diagonal of the Mo_4 square. In the $6a_{1g}$ orbital, the mixing of $5p_z$ and $4d_{z^2}$ orbitals is apparent, resulting in hybrid orbitals that are directed away from the radial chlorine atoms. This hybridization reduces the Mo–Cl antibonding interaction and strengthens the Mo–Mo σ-bonding in the orbital. The competition for use of Mo $4d_{z^2}$ and $5p_z$ atomic orbitals for σ-bonding is a simple orbital picture of a mutual trans influence between metal–metal cluster bonding and radial metal–ligand bonding, i.e. the *radial cluster influence*. Similar interactions have been seen previously in theoretical studies of the radial Re–Cl bonds of $Re_3Cl_{12}^{3-}$,[23] the radial Zr–I bonds in the closo octahedral clusters of formula $Zr_6I_{12}^{2+}$ and $Zr_6I_{18}^{4-}$,[24] and even the radial (axial) metal–ligand bonds in $M_2(O_2CH)_4L_2$ compounds.[25-27] Contour diagrams of the $5b_{2g}$ and $8e_u$ Mo–Mo σ-bonding levels of $Mo_4(\mu_2\text{-}OH)_8Cl_4$ are shown in Figure 5, and these can be compared to the qualitative drawings of metal–metal b_{2g} and e_u orbitals in III. For the complete $Mo_4(\mu_2\text{-}OH)_8Cl_4$

(23) Bursten, B. E.; Cotton, F. A.; Green, J. C.; Seddon, E. A.; Stanley, G. G. *J. Am. Chem. Soc.* **1980**, *102*, 955.
(24) Smith, J. D.; Corbett, J. D. *J. Am. Chem. Soc.* **1985**, *107*, 5704.
(25) Norman, J. G., Jr.; Kolari, H. J. *J. Am. Chem. Soc.* **1978**, *100*, 791.
(26) Norman, J. G., Jr.; Renzoni, G. E.; Case, D. A. *J. Am. Chem. Soc.* **1979**, *101*, 5256.
(27) Bursten, B. E.; Cotton, F. A. *Inorg. Chem.* **1981**, *20*, 3042.

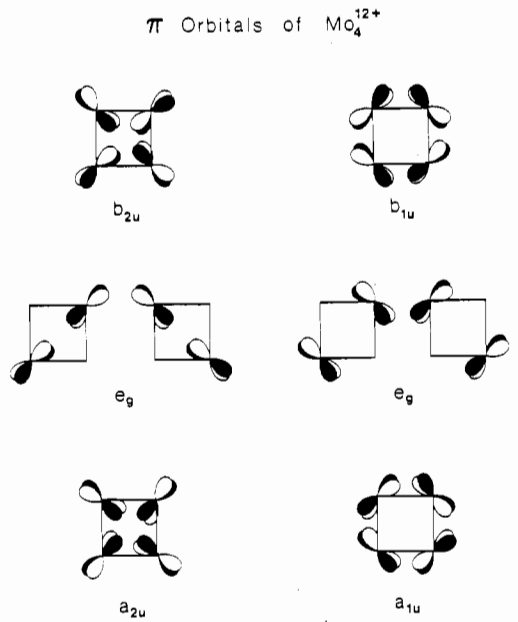

Figure 6. The eight framework π-bonding (plane antisymmetric) orbitals of Mo_4^{12+} constructed from metal d_{yz} (left) and d_{xy} (right) atomic orbitals.

cluster, it is seen that, of the 12 valence electrons expected for Mo, 10 occupy the $6a_{1g}$, $8e_u$, $5b_{2g}$, and $7a_{1g}$ Mo–Mo σ-bonding orbitals and two occupy the $4a_{2u}$ Mo–Mo π-bonding orbital. This suggests a rather interesting parallel between the π-bonding orbitals of D_{4h} $Mo_4(\mu_2\text{-}X)_8X_4$ clusters and those of square cyclobutadiene, which we will now address.

$Mo_4(\mu\text{-}X)_8X_4$: Inorganic Cyclobutadiene? Under D_{4h} symmetry the $p\pi$ orbitals of square cyclobutadiene transform as the $a_{2u} + e_g + b_{2u}$ irreducible representations. By contrast, two d orbitals, d_{xy} and d_{yz}, are plane-antisymmetric in Mo_4^{12+} and transform under D_{4h} symmetry as $a_{1u} + a_{2u} + b_{1u} + b_{2u} + 2e_g$ irreducible representations. These eight $d\pi$ orbitals of Mo_4^{12+} are illustrated schematically in Figure 6. The set of d orbitals derived from d_{xy} atomic orbitals ($a_{1u} + e_g + b_{1u}$), shown on the right in Figure 6, are all directed at the sites of the incoming bridging ligands and are removed from the frontier region by interaction to form $Mo_4(\mu_2\text{-}X)_8Cl_4$ ($X = Cl^-$, OH^-). Thus, for $Mo_4(\mu_2\text{-}X)_8Cl_4$ clusters, only the $d\pi$ orbitals on the left of Figure 6 survive the perturbations imposed by the bridging ligands. The a_{2u} $d\pi$ orbitals correspond to the HOMO and the e_g $d\pi$ orbitals correspond to the LUMO of $Mo_4(\mu_2\text{-}OH)_8Cl_4$. A comparison of framework π orbitals of cyclobutadiene and $Mo_4(\mu_2\text{-}OH)_8Cl_4$ is illustrated in Figure 7. Although both cyclobutadiene and Mo_4^{12+} have four π electrons, the situation changes in the presence of bridging ligands. Whereas square cyclobutadiene is expected to have two electrons in both the a_{2u} and e_g π-orbitals, $Mo_4(\mu_2\text{-}OH)_8Cl_4$ has only the a_{2u} orbital occupied. The e_g orbital is the LUMO, and thus $Mo_4(\mu_2\text{-}OH)_8Cl_4$ cannot be considered as "inorganic cyclobutadiene". The primary difference between these systems arises from the bonding capabilities of d vs p orbitals, which allows for a greater number of σ and π orbitals in $Mo_4(\mu_2\text{-}X)_8Cl_4$ than in square cyclobutadiene. As a consequence, square $Mo_4(\mu_2\text{-}X)_8Cl_4$ has 10 electrons in Mo–Mo σ-bonding orbitals whereas square cyclobutadiene has only 8 electrons in C–C σ-bonding orbitals. The analogy in the π orbitals of cyclobutadiene and the $Mo_4(\mu_2\text{-}OH)_8Cl_4$ cluster is intriguing in that cyclobutadiene has been both predicted[28–33] and shown experimentally[34–36] to be subject to Jahn–Teller distortions,

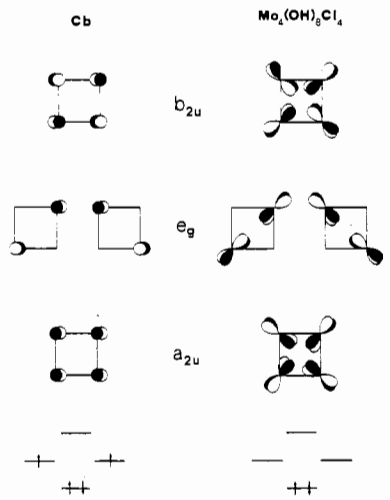

Figure 7. Comparison of the four framework π-bonding orbitals of D_{4h} cyclobutadiene (Cb; left) and $Mo_4(\mu\text{-}OH)_8Cl_4$ (right). The HOMO's of each are denoted by arrows at the bottom.

resulting in a nonsquare equilibrium geometry. Thus, one might anticipate that if more electrons could be introduced into the e_g LUMO of $Mo_4(\mu_2\text{-}X)_8Cl_4$, a Jahn–Teller distortion would result in direct analogy with cyclobutadiene.

This analysis seems consistent with the structure of the chloromolybdate ion $Mo_4(\mu_2\text{-}Cl)_8Cl_4^{3-}$ reported by McCarley and Aufdembrink,[3] i.e. a rectangular cluster with a slight rhombic distortion. We have chosen to investigate the possible distortion of this cluster from a square equilibrium geometry by first introducing three more electrons into the square cluster to yield D_{4h} $Mo_4(\mu_2\text{-}Cl)_8Cl_4^{3-}$. Next we examine the electronic structure of an idealized D_{2h} rectangular $Mo_4(\mu_2\text{-}Cl)_8Cl_4^{3-}$ cluster and look for a correlation between the molecular orbitals of D_{4h} and D_{2h} symmetry.

Jahn–Teller Distortions in D_{4h} Tetranuclear Mo Clusters. Using the D_{4h} $Mo_4(\mu_2\text{-}Cl)_8Cl_4$ cluster as the example, we observe that introduction of either one or three electrons into the e_g nonbonding LUMO to give D_{4h} $Mo_4(\mu_2\text{-}Cl)_8Cl_4^-$ or $Mo_4(\mu_2\text{-}Cl)_8Cl_4^{3-}$ will result in electronic configurations of $|...a_{2u}^2e_g^1\rangle$ or $|...a_{2u}^2e_g^3\rangle$, both of which lead to a degenerate ^2E_g state. According to the Jahn–Teller theorem,[37,38] a degenerate ground state in a 4-fold symmetric system of D_{4h} symmetry will lead to distortions along normal modes of b_{1g} or b_{2g} symmetry to remove the degeneracy.[39] These Jahn–Teller-active vibrations are shown in IV, and both will distort

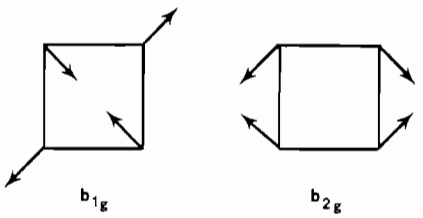

IV

(28) Buenker, R. J.; Peyerimhoff, S. D. *J. Chem. Phys.* **1968**, *48*, 354.
(29) Dewar, M. J. S.; Kohn, M. C.; Trinajstic, N. *J. Am. Chem. Soc.* **1971**, *93*, 3437.
(30) Kollmar, H.; Stammler, V. J. *J. Am. Chem. Soc.* **1977**, *99*, 3583.
(31) Jafri, J. A.; Newton, M. J. *J. Am. Chem. Soc.* **1978**, *100*, 5012.
(32) Borden, W. T.; Davidson, E. R.; Hart, P. *J. Am. Chem. Soc.* **1978**, *100*, 388.
(33) Borden, W. T.; Davidson, E. R. *Acc. Chem. Res.* **1981**, *14*, 69.
(34) Masamune, S.; Sonto-Bachiller, F. A.; Machinguchi, T.; Bertie, J. E. *J. Am. Chem. Soc.* **1978**, *100*, 4889.
(35) Whitman, D. W.; Carpenter, B. K. *J. Am. Chem. Soc.* **1980**, *102*, 4272.
(36) Balley, T.; Masamune, S. *Tetrahedron* **1980**, *36*, 343.
(37) Jahn, H. A.; Teller, E. *Proc. R. Soc. London, Ser. A* **1937**, *161*, 220.
(38) Many examples of the Jahn–Teller theorem have been discussed in the literature. Two very good books include: (a) Engleman, R. *The Jahn-Teller Effect in Molecules and Crystals*; Wiley-Interscience: New York, 1972. (b) Bersuker, I. B. *The Jahn-Teller Effect and Vibronic Interactions in Modern Chemistry*; Plenum: New York, 1984. (c) For an excellent discussion see: Pearson, R. G. *Proc. Natl. Acad. Sci. U.S.A.* **1975**, *72*, 2104.
(39) The 4-fold symmetry problem has been lucidly discussed. See for example: (a) Bacci, M. *Phys. Rev. B: Condens. Matter* **1978**, *17*, 4495. (b) Child, M. S. *Mol. Phys.* **1960**, *3*, 601. (c) Hougen, J. T. *J. Mol. Spectrosc.* **1964**, *13*, 149. (d) Ballhausen, C. J. *Theor. Chim. Acta* **1965**, *3*, 368.

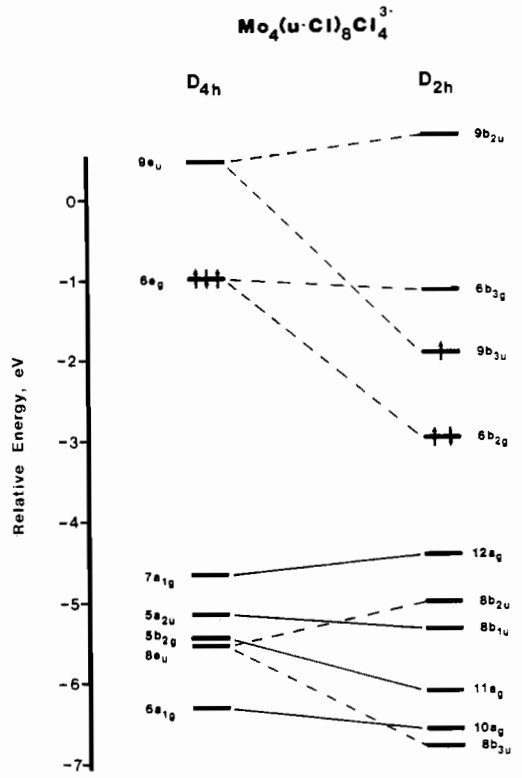

Figure 8. Correlation diagram comparing the relative orbital energies of $Mo_4(\mu\text{-}Cl)_8Cl_4^{3-}$ in D_{4h} (left) and D_{2h} (right) geometries. Solid lines trace nondegenerate orbitals from D_{4h} to D_{2h} symmetry, and dashed lines connect degenerate orbitals in D_{4h} symmetry to their two nondegenerate counterparts in D_{2h} symmetry. The HOMO's of each geometry are denoted by arrows.

the D_{4h} square cluster into D_{2h} symmetry. The b_{1g} mode will produce a rhomboidal distortion, and the b_{2g} mode will produce a rectangular distortion. The Jahn–Teller theorem and group-theoretical considerations mandate that in such a situation the cluster *must* distort to remove the electronic degeneracy, and it is known a priori that the square structure will be unstable.

In the case of square cyclobutadiene and its radical cation, sophisticated electronic structure calculations predict the rectangular distortion to yield the lowest energy geometry.[33,40,41] In the case of square $Mo_4Cl_{12}^{3-}$, it is not possible for us to use the Fenske–Hall method to determine which distorted structure will have the lowest energy. However, we can use the Fenske–Hall method as a tool toward rationalizing the rectangular geometry of $Mo_4Cl_{12}^{3-}$ as the result of a first-order Jahn–Teller instability in the more symmetrical D_{4h} square structure.

It is clear that a rectangular distortion of the regular D_{4h} cluster to give the D_{2h} chloromolybdate ion is a feasible means of lifting the degeneracy of the e orbitals, thereby removing the electronic degeneracy. Figure 8 shows the one-to-one correspondence between the molecular orbitals of the D_{4h} and D_{2h} $Mo_4(\mu_2\text{-}Cl)_8Cl_4^{3-}$ clusters. Solid lines trace nondegenerate orbitals from D_{4h} to D_{2h} symmetry, and dashed lines connect degenerate orbitals in D_{4h} symmetry to their two nondegenerate counterparts in D_{2h} symmetry. When the difference between the short and long Mo–Mo bonds becomes great enough, the distortion is actually seen to be symmetry forbidden as the $9b_{3u}$ HOMO in the D_{2h} geometry originates from the $9e_u$ LUMO in D_{4h} symmetry, although the inherent barrier should be quite small. To help amplify the fact that there exists a direct one-to-one correspondence to orbital shapes from higher to lower symmetry, representative contour diagrams of selected pairs of D_{4h} and D_{2h} cluster orbitals are shown

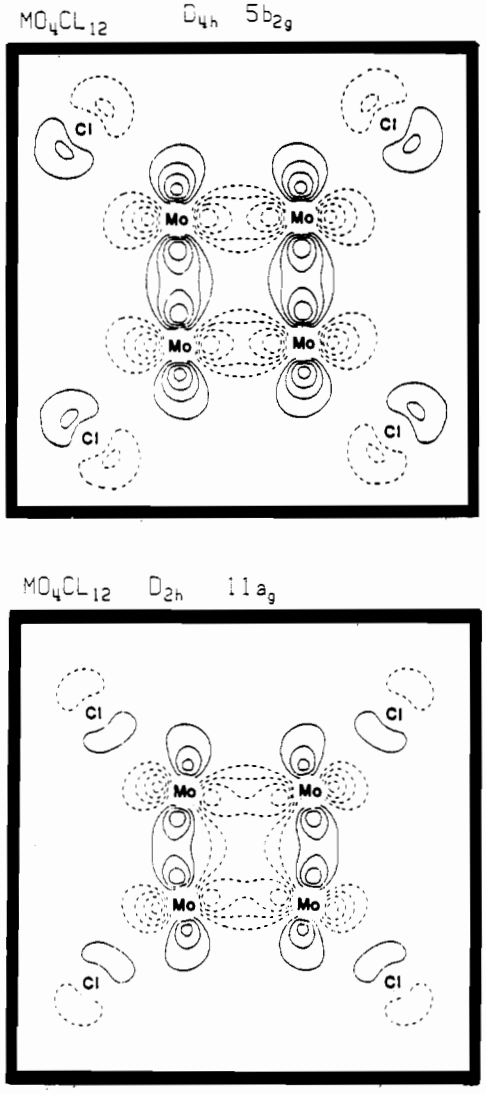

Figure 9. Contour plots comparing the $5b_{2g}$ orbital of D_{4h} symmetry (top) to the $11a_g$ orbital of D_{2h} symmetry (bottom) for $Mo_4(\mu\text{-}Cl)_8Cl_4^{3-}$. This plot is taken in the Mo_4 plane containing the four Mo and four radial chlorine atoms.

in Figures 9 and 10. The similarity of the orbitals under the two geometries is inescapable, and thus, it is concluded that the rectangular geometry of the chloromolybdate ion $Mo_4(\mu_2\text{-}Cl)_8Cl_4^{3-}$ can be viewed as a result of a first-order Jahn–Teller instability in the more symmetric D_{4h} square structure.

(2) Halide- and Alkoxide-Supported Mo_4 Butterfly Clusters. Due to the low symmetry of the C_{2v} Mo_4 butterfly structures found for $Mo_4(\mu_3\text{-}O\text{-}i\text{-}Pr)_2(\mu_2\text{-}O\text{-}i\text{-}Pr)_4(O\text{-}i\text{-}Pr)_2Br_4$, $Mo_4(\mu_3\text{-}Cl)_2(\mu_2\text{-}Cl)_4Cl_6^{3-}$, and $Mo_4(\mu_3\text{-}I)_2(\mu_2\text{-}I)_5I_4^{2-}$, the "clusters-in-molecules" approach toward understanding the bonding in this geometry is not nearly so straightforward as it was for the more symmetrical square and rectangular clusters. Nevertheless, the approach does reveal much useful information regarding the role of various ligand types and is therefore adopted.

The C_{2v} Mo_4^{12+} Cluster Core. Due to the complexity of the C_{2v} Mo_4 butterfly geometry, it is most convenient to introduce the metal–metal framework-bonding orbitals of C_{2v} Mo_4^{12+} in the form of orbital pictures. The 12 molybdenum 4d electrons are expected to occupy the $1a_1$, $1b_2$, $2a_1$, $1b_1$, $1a_2$, and $3a_1$ metal–metal framework-bonding orbitals of C_{2v} Mo_4^{12+} shown qualitatively in V. As we did earlier, we have examined the bonding of the C_{2v} Mo_4^{12+} core with each type of ligand set separately in order to avoid having to sort out those effects due to the other ligands. For each ligand set, the canonical orbitals of C_{2v} Mo_4^{12+} are destabilized by interaction with the ligands, and the magnitude of destabilization can be taken as a rough measure of the stabilizing interaction occurring in lower lying bonding orbitals. Using this

(40) Borden, W. T.; Davidson, E. R.; Feller, D. *J. Am. Chem. Soc.* **1981**, *103*, 5725.

(41) For an excellent discussion and summary of the cyclobutadiene radical cation and neutral molecule see: Davidson, E. R.; Borden, W. T. *J. Chem. Phys.* **1983**, *87*, 4783.

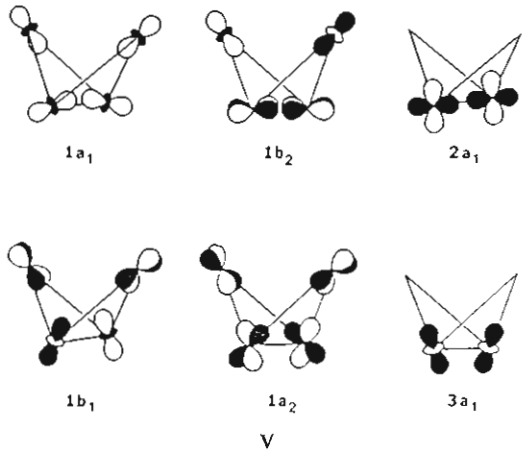

V

approach in conjunction with the Mulliken populations of the canonical orbitals of C_{2v} Mo_4^{12+} for each ligand set, it is possible to order the ligand sets according to their influence on the C_{2v} Mo_4^{12+} core. The general ordering obtained from such analyses can be summarized as

$$(\mu_3\text{-L})_2^{2-} > (\mu_2\text{-L})_4^{4-} > L_6^{6-}$$

This ordering is merely an extension of our earlier studies, namely that the capping ligands influence the cluster core the most, followed by the bridging ligands, and the terminal ligands influence the cluster core the least. The overall effects of the capping (μ_3-L), edge-bridging (μ_2-L), and terminal ligand sets on the C_{2v} Mo_4^{12+} framework show a remarkable parallel to the effects of the same ligand sets on an equilateral triangular cluster.[19] This should not be too surprising since the butterfly geometry may be regarded as two equilateral triangles fused along a common edge. In the same fashion that the $Mo_4(\mu_3\text{-X})_2(\mu_2\text{-X})_4X_6$ cluster may be regarded as an arachno derivative of the *closo*-$Mo_6(\mu_3\text{-X})_8X_6^{2-}$ cluster, one could envision a hypho derivative of formula $Mo_3(\mu_3\text{-X})(\mu_2\text{-X})_3X_6$. We will use this comparison between triangular and butterfly geometries as a pedagogical aid for interpreting the pronounced influence of capping ligands on the C_{2v} Mo_4^{12+} butterfly core.

Pronounced Influence of Capping Ligands. The question of how capping ligands influence the central Mo_4^{12+} butterfly framework will be addressed by first investigating the effect of a single capping ligand on the central core of an equilateral triangle and then comparing it to the effect of capping ligands on the central core of the butterfly framework. To more simply illustrate how the capping ligands perturb the central core, we have performed calculations for $Mo_3(\mu_3\text{-OH})^{9+}$ and transformed the results into a basis consisting of the canonical orbitals of Mo_3^{10+}. The complete results for the trinuclear cluster fragments are not reported here, for they are essentially the same as those reported earlier.[19,20] Unlike the situation for the earlier studies, our primary interest is in the effect of a single capping ligand, and hence we will treat the trinuclear cluster core under C_{3v} symmetry. When the symmetry is lowered from D_{3h} to C_{3v}, the symmetry or antisymmetry about the horizontal mirror plane is lost, giving rise to results slightly different from those previously reported for two capping ligands.[19,20] For a single capping OH^- ligand we find a strong bonding interaction between the OH^- σ lone-pair orbital and Mo_3^{12+} orbitals of a_1 symmetry. The $1a_1$, $2a_1$, and $3a_1$ orbitals of Mo_3^{10+} important to our discussion are illustrated qualitatively in VI. With use of a local coordinate system on each metal atom

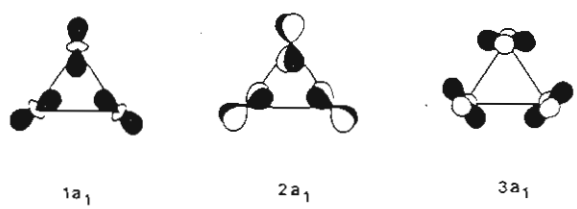

VI

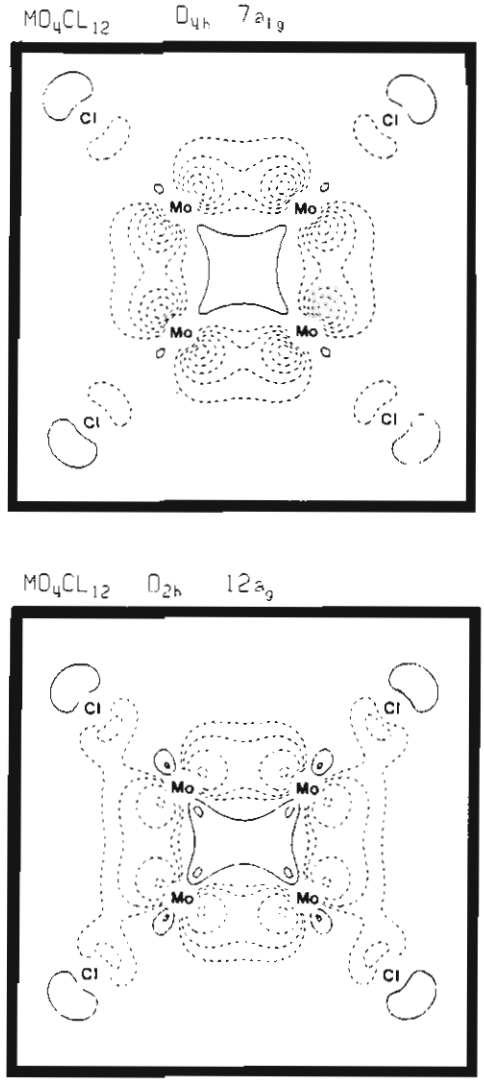

Figure 10. Contour plots comparing the $7a_{1g}$ orbital of D_{4h} symmetry (top) to the $12a_g$ orbital of D_{2h} symmetry (bottom) for $Mo_4(\mu\text{-Cl})_8Cl_4^{3-}$.

in the triangle with radial z, tangential x, and perpendicular y axes, the $1a_1$, $2a_1$, and $3a_1$ orbitals may be regarded as the all-in-phase combinations of Mo $4d_{z^2}$, $4d_{yz}$, and $4d_{x^2-y^2}$ atomic orbitals, respectively. It is noted that the fusing of two triangles along a common edge could transform the $1a_1$ orbital of Mo_3^{10+} (shown in VI) into the $1a_1$ orbital of the Mo_4^{12+} butterfly (shown in V) and so on.

The most favorable interaction between the σ orbital of a single capping OH^- ligand and the Mo_3^{10+} triangle can be achieved via mixing of the $1a_1$ and $2a_1$ cluster orbitals to generate hybrid orbitals that are directed toward and away from the capping ligand. In order to allow the hybrid orbital that is directed toward the ligand to act as an acceptor of charge, the hybridization is accompanied by the formal promotion of the electrons that were in the $2a_1$ orbital up to the $3a_1$ orbital. This is illustrated in the MO diagram shown in Figure 11, and the resultant hybrids, and their interactions with the σ orbital of the capping ligand, are depicted qualitatively in VII. It can be seen from the MO

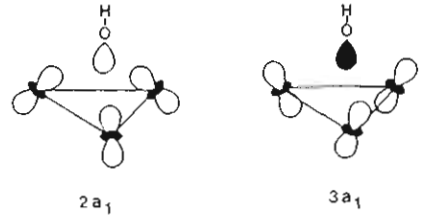

VII

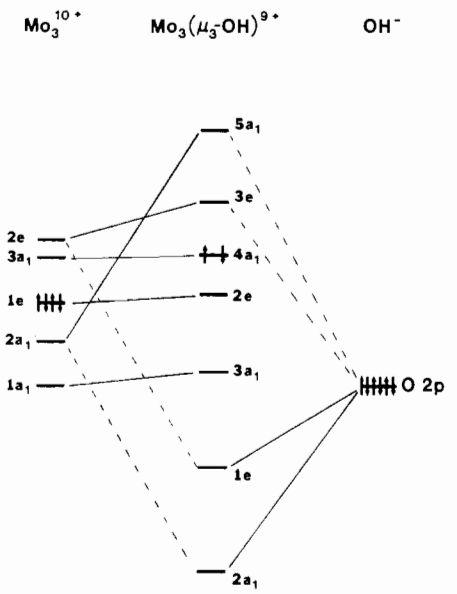

Figure 11. Correlation diagram showing the interaction of primarily metal–metal bonding orbitals of Mo_3^{10+} with a single capping μ_3-OH ligand. The HOMO's of each fragment are denoted by arrows.

Table III. Mulliken Populations of the Canonical Orbitals of C_{3v} Mo_3^{10+} for $[Mo_3(\mu_3\text{-}OH)]^{9+}$

orbital	Mo_3^{10+}	$[Mo_3(\mu_3\text{-}OH)]^{9+}$	orbital	Mo_3^{10+}	$[Mo_3(\mu_3\text{-}OH)]^{9+}$
$1a_1$	2.00	1.77	3e	0.00	0.39
$2a_1$	2.00	0.95	4e	0.00	0.00
1e	4.00	3.86	5e	0.00	0.04
$3a_1$	0.00	1.86	$1a_2$	0.00	0.00
2e	0.00	0.72			

diagram that the primary a_1 σ-interaction to give $Mo_3(\mu_3\text{-}OH)^{9+}$ results in one strong metal–ligand bonding orbital ($2a_1$), one metal–ligand nonbonding orbital ($3a_1$), and one metal–ligand antibonding orbital ($5a_1$). The $3a_1$ orbital is slightly tipped out of the metal plane, and thus some metal–metal bonding is sacrificed to facilitate metal–ligand bonding, yet the lion's share of metal–metal cluster bonding is preserved in spite of this interaction. A secondary interaction occurs between Mo_3^{10+} orbitals and the OH^- pπ orbitals, which have e symmetry. This secondary metal–ligand bonding occurs via donation from capping-ligand π lone-pair orbitals into the unoccupied 2e orbitals of the Mo_3^{10+} cluster, as can be seen in Figure 11.

The effects of the a_1 and e metal–ligand bonding interactions on metal–metal cluster-bonding orbitals are further amplified by examination of the Mulliken populations of the canonical orbitals of Mo_3^{10+} in $Mo_3(\mu_3\text{-}OH)^{9+}$ given in Table III. From the table it is clear that the capping ligand effects the transfer of charge out of the $2a_1$ orbital of Mo_3^{10+} and into the $3a_1$ orbital. In a similar fashion, the populations indicate that the capping ligand has little effect on the population of the 1e orbital and that the 2e orbital of Mo_3^{10+} acts as a charge acceptor. These effects seen for the C_{3v} $Mo_3(\mu_3\text{-}OH)^{9+}$ fragment are very similar to those previously discussed for the C_{3v} $Mo_3(\mu_3\text{-}O)(\mu_2\text{-}O)_3^{4+}$ fragment, wherein it was also seen that the capping ligand forced a rehybridization of the Mo–Mo cluster-bonding orbitals.[19]

Ligand Preference. In this section we will consider the bonding in halide- and alkoxide-supported C_{2v} butterfly clusters of general formula $Mo_4(\mu_3\text{-}X)_2(\mu_2\text{-}X)_4X_2Cl_4$, where X = Cl^- and OH^-. We will begin by applying the perturbations of each ligand set in our established order of influence on the central Mo_4^{12+} core. For X = OH^-, Figure 12 shows the correlation of energy levels of Mo_4^{12+}, $Mo_4(\mu_3\text{-}OH)_2^{10+}$, $Mo_4(\mu_3\text{-}OH)_2(\mu_2\text{-}OH)_4^{6+}$, and the complete $Mo_4(OH)_8Cl_4$ cluster. Table IV lists the Mulliken populations of the canonical orbitals of C_{2v} Mo_4^{12+} for each independent ligand set and degree of perturbation and can be used to help understand the correlation diagram and ordering of ligand

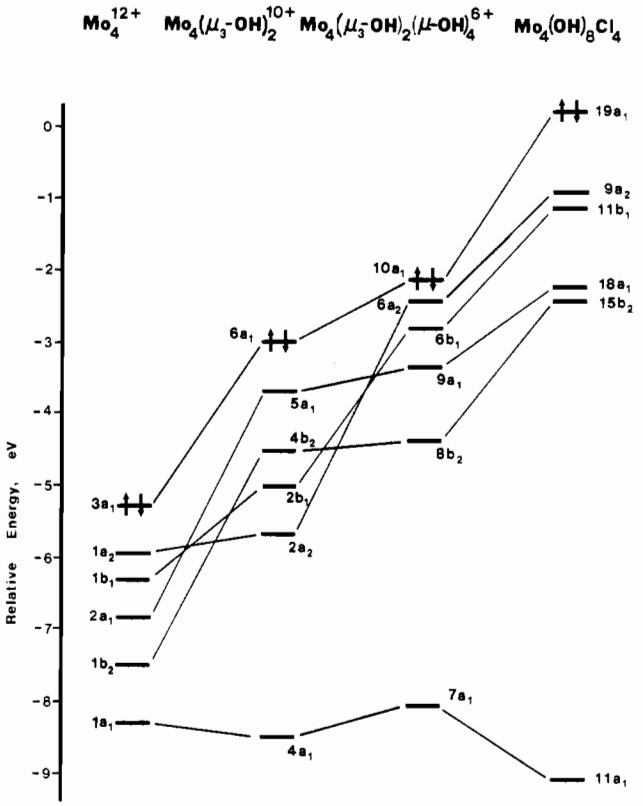

Figure 12. Correlation diagram tracing the perturbation of primarily metal–metal bonding orbitals of C_{2v} Mo_4^{12+} (left) as ligation occurs through (1) interaction with two μ_3-OH ligands (second column from left), (2) interaction with four μ_2-OH ligands (third column from left), and (3) interaction with terminal OH and four radial Cl ligands (far right). The HOMO for each degree of perturbation is denoted by arrows.

sets. As was the case for the Mo_3 triangle, the set of capping ligands has a primary σ- and secondary π-interaction with the Mo_4^{12+} framework-bonding orbitals. The primary interaction between the capping ligands and Mo_4^{12+} is with the set of $(\mu_3\text{-}X)_2^{2-}$ σ lone-pair orbitals which span the $a_1 + b_2$ irreducible representations. The correlation diagram shown in Figure 12 for X = OH^- shows that, as expected, Mo_4^{12+} orbitals of a_1 and b_2 symmetry are destabilized the most as a result of interaction with capping ligands. Once again, the set of capping ligands forces a rehybridization of the a_1 cluster orbitals and the resulting hybrid orbitals are tipped out of the metal plane. This is precisely the type of interaction seen in the Mo_3 triangle, although the rehybridization has more important ramifications toward cluster bonding in the butterfly geometry. We illustrate the $1a_1$ orbital of Mo_4^{12+} and its rehybridized $4a_1$ counterpart in $Mo_4(\mu_3\text{-}OH)_2^{10+}$ in VIII. There is relatively little loss of metal–metal overlap in

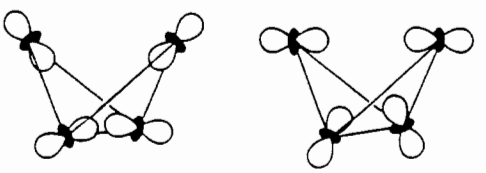

VIII

the a_1 cluster-bonding orbital as a result of interaction with the capping-ligand set. Indeed, it can be seen from the correlation diagram of Figure 12 that the $1a_1$ orbital of C_{2v} Mo_4^{12+} is not destabilized by interaction with any of the ligands.

A secondary π-interaction occurs between Mo_4^{12+} and the $(\mu_3\text{-}X)_2^{2-}$ pπ lone-pair orbitals, which span the $a_1 + a_2 + b_1 + b_2$ representations. This π-interaction not only contributes to the destabilization of a_1 and b_2 cluster-bonding orbitals but also forces

Table IV. Mulliken Populations of the Canonical Orbitals of C_{2v} Mo_4^{12+} for $Mo_4(\mu_3\text{-}X)_2^{10+}$, $Mo_4(\mu_2\text{-}X)_4^{8+}$, $Mo_4(\mu_3\text{-}X)_2(\mu_2\text{-}X)_4^{6+}$, and $Mo_4X_8Cl_4$, Where X = Cl^-, OH^-

		$Mo_4(\mu_3\text{-}X)_2^{10+}$		$Mo_4(\mu_2\text{-}X)_4^{8+}$		$Mo_4(\mu_3\text{-}X)_2(\mu_2\text{-}X)_4^{6+}$		$Mo_4X_8Cl_4$	
orbital	Mo_4^{12+}	X = Cl	X = OH	X = Cl	X = OH	X = Cl	X = OH	X = Cl	X = OH
$1a_1$	2.00	1.94	1.96	1.93	1.91	1.96	1.95	1.97	1.96
$1b_2$	2.00	1.53	1.34	1.95	1.96	1.57	1.55	1.62	1.60
$2a_1$	2.00	1.71	1.68	1.91	1.87	1.65	1.61	1.63	1.62
$1a_2$	2.00	1.97	1.98	1.77	1.58	1.76	1.62	1.80	1.62
$1b_1$	2.00	1.24	1.45	1.74	1.60	1.60	1.49	1.67	1.54
$3a_1$	2.00	1.64	1.63	1.85	1.84	1.59	1.52	1.63	1.79
$2b_2$	0.00	1.52	1.24	1.20	0.66	1.08	0.82	0.99	0.74
$2b_1$	0.00	1.48	1.25	0.91	0.91	0.80	0.51	0.83	0.79
$4a_1$	0.00	0.74	0.69	0.50	0.58	0.63	0.65	0.63	0.54
$3b_2$	0.00	0.35	0.17	0.59	0.16	0.86	0.71	0.74	0.70
$2a_2$	0.00	0.35	0.19	1.08	0.59	0.83	0.56	0.51	0.59
$5a_1$	0.00	0.78	0.79	0.10	0.25	0.89	0.78	0.86	0.80
$6a_1$	0.00	0.39	0.11	0.21	0.09	0.64	0.69	0.53	0.48
$3a_2$	0.00	0.05	0.11	0.94	0.91	0.99	0.89	0.83	0.79

a destabilization and mixing of b_1 orbitals.

The combined σ- and π-interactions of the capping ligands with the Mo_4^{12+} core are also seen in the Mulliken populations of the canonical orbitals of C_{2v} Mo_4^{12+} in $Mo_4(\mu_3\text{-}X)_2^{10+}$ species (Table IV). The table reveals that the capping ligands favor the transfer of charge out of the $1b_2$, $2a_1$, $1b_1$, and $3a_1$ orbitals and into the $2b_2$, $2b_1$, $4a_1$, and $5a_1$ orbitals as a result of both σ- and π-interactions. Similarly, the table emphasizes that the $1a_1$ and $1a_2$ orbitals of Mo_4^{12+} are scarcely affected by the capping ligands as indicated by the negligible decreases in their Mulliken populations.

As was the case for the square Mo_4 systems, the edge-bridging ligands and the capping ligands interact with different orbitals of Mo_4^{12+}. The Mulliken populations of C_{2v} Mo_4^{12+} orbitals in $Mo_4(\mu_2\text{-}X)_4^{8+}$ species reveal that the edge-bridging ligands have only a small effect on the populations of the $1a_1$, $1b_2$, and $2a_1$ orbitals of Mo_4^{12+} and favor instead the transfer of charge out of the $1a_2$, $1b_1$, and $3a_1$ orbitals, with the $2b_2$, $2b_1$, $2a_2$, and $3a_2$ orbitals acting as charge acceptors. These acceptor orbitals are all directed at the site of the incoming edge-bridging donors and are energetically raised out of the frontier region upon the formation of $Mo_4(\mu_2\text{-}X)_4^{8+}$. Also, in complete analogy to the square and triangular systems, when both capping and edge-bridging ligands are present as in $Mo_4(\mu_3\text{-}X)_2(\mu_2\text{-}X)_4^{6+}$, the ligand influence on the Mo_4^{12+} fragment is dominated by the capping ligands. From an analysis identical with that used above, we deduce the general ordering of ligand sets to be

$$(\mu_3\text{-}X)_2^{2-} > (\mu_2\text{-}X)_4^{4-} > (\text{terminal})_6^{6-}$$

A close examination of Table IV indicates that, as was the case for the square clusters, OH^- ligands have a greater destabilizing influence on the Mo_4^{12+} core than do Cl^- ligands inasmuch as the OH^- ligands favor a greater transfer of charge out of the canonical orbitals of Mo_4^{12+}. From this we can deduce a further breakdown in the general ordering of ligand sets:

$$(\mu_3\text{-}OH)_2^{2-} > (\mu_3\text{-}Cl)_2^{2-}$$

$$(\mu_2\text{-}OH)_4^{4-} > (\mu_2\text{-}Cl)_4^{4-}$$

and finally

$$(\mu_3\text{-}OH)_2^{2-} > (\mu_2\text{-}OH)_4^{4-} > (\mu_2\text{-}Cl)_4^{4-} > (\text{terminal})_6^{6-}$$

This final ordering is quite satisfying since, in the characterized alkoxide-supported clusters of formula $Mo_4(\mu_3\text{-O-}i\text{-Pr})_2(\mu_2\text{-O-}i\text{-Pr})_4(\text{O-}i\text{-Pr})_2X_4$, the alkoxide ligands preferentially occupy capping and bridging positions over the halide.[1,2]

For both the square and butterfly complexes, we have seen that an alkoxide ligand has a stronger interaction with the metal–metal framework-bonding orbitals than does a halide ligand in the same bonding mode. We attribute this to the energetic difference between O 2p and Cl 3p atomic orbitals relative to the Mo 4d orbitals and to the magnitude of the atomic orbital overlaps. Although the Mo 4d–Cl 3p energy gap is smaller than the Mo 4d–O 2p gap, the ⟨Mo 4d|Cl 3p⟩ overlap is smaller than ⟨Mo 4d|O 2p⟩, largely because of the longer Mo–Cl bond and more diffuse valence orbitals. In addition, 2s–2p orbital mixing can and does occur in the σ lone pair orbital of OH^-, further accentuating the overlap with the metal AO's. As a consequence, the alkoxide ligand is the better donor to molybdenum and preferentially occupies the bridging sites over the halide ligand in mixed halo–alkoxy clusters.

Metal–Metal Bonding and the Radial Cluster Influence. Now that we have firmly established the effects of the various ligand sets on the central Mo_4^{12+} butterfly core, we are in a position to take a closer look at the metal–metal bonding in the complete $Mo_4(\mu_3\text{-}X)_2(\mu_2\text{-}X)_4X_6$ cluster. The occupied molecular orbitals of the model cluster $Mo_4(\mu_3\text{-OH})_2(\mu_2\text{-OH})_4(OH)_2Cl_4$ that are primarily involved in metal–metal cluster bonding are illustrated in IX. The 12 metal-based electrons occupy the $11a_1$, $15b_2$, $18a_1$, $11b_1$, $9a_2$, and $19a_1$ orbitals shown in IX, and their relative orbital energetics are shown in Figure 12. Although all of these orbitals are metal–metal bonding, the nature of the bonding varies considerably. For example, the $15b_2$ orbital is bonding between the "wingtip" and "backbone" molybdenum atoms and is delocalized across the faces and edges of the triangles formed by the backbone and wingtip atoms. The $11b_1$ and $9a_2$ orbitals are also bonding between wingtip and backbone molybdenum atoms, but the bonds are concentrated along the four edges of the butterfly. The $18a_1$ and $19a_1$ orbitals are both localized in the backbone molybdenum atoms, but the $19a_1$ orbital does have some contribution from the wingtip atoms in a nonbonding fashion. These same orbitals are found for the chloride-supported cluster $Mo_4(\mu_3\text{-Cl})_2(\mu_2\text{-Cl})_4Cl_6$ except that a more pronounced degree of metal–ligand mixing is seen in the orbitals and this exactly parallels that previously discussed for the D_{4h} square clusters. For the 15-electron chloromolybdate ion of formula $Mo_4(\mu_3\text{-Cl})_2(\mu_2\text{-Cl})_4Cl_6^{3-}$, the additional three electrons occupy the $12b_1$ and $10a_2$ orbitals, which are illustrated in X. The $12b_1$ orbital is primarily localized in the backbone molybdenum atoms and is weakly antibonding across the backbone but bonding across the wingtip. At shorter wingtip–wingtip separations, such as that found for the 15-electron

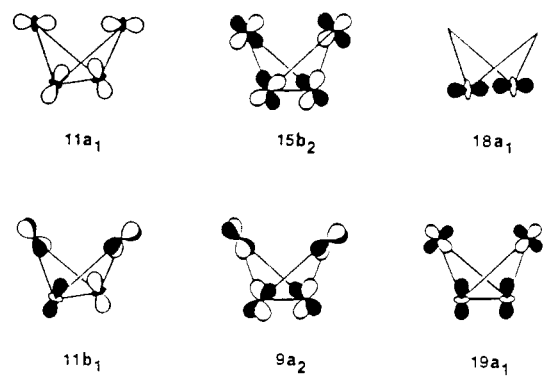

IX

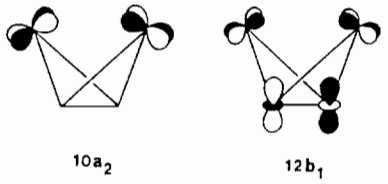

X

iodo-bridged cluster $Mo_4(\mu_3\text{-}I)_2(\mu_2\text{-}I)_5I_4^{2-}$, the $12b_1$ orbital drops below the $19a_1$ orbital owing to the increased bonding interaction between wingtip atoms at the shorter "wingspan", as has been previously discussed by Johnston and Mingos.[17] The $10a_2$ orbital is the HOMO for 15-electron clusters, is localized on the wingtip atoms, and is weakly antibonding. Contour plots of the backbone-localized HOMO and LUMO of $Mo_4(\mu_3\text{-}OH)_2(\mu_2\text{-}OH)_4(OH)_2Cl_4$ are shown in Figure 13.

The butterfly clusters just discussed show further evidence of the *radial cluster influence*. This phenomenon is anticipated since these clusters represent alternate arachno structures of the closo Mo_6 octahedral cluster. Its presence in the Mo_4 butterfly clusters can be seen in contour plots of selected orbitals of the complex. The $7b_1$ orbital shown in Figure 14 is the b_1 Mo–Cl σ-bonding orbital of $Mo_4(OH)_8Cl_4$, and $11b_1$ (also shown in Figure 14) is its rehybridized Mo–Cl σ-antibonding counterpart. Recall that the $11b_1$ orbital, as shown in IX, is metal–metal σ-bonding along the four edges of the butterfly and antibonding between backbone atoms. The contour plot in Figure 14 is shown in the plane containing the backbone Mo atoms and two radial Cl ligands and emphasizes the Mo–Cl σ-antibonding interaction (rather than the Mo–Mo bonding) in an occupied MO. Figure 15 illustrates that the $11a_1$ orbital is both Mo–Mo and Mo–Cl σ-bonding, while $17a_1$ is the corresponding Mo–Mo σ-bonding and Mo–Cl σ-antibonding counterpart.

Concluding Remarks

This work has demonstrated that an intimate relationship exists between the electronic structures of square, rectangular, and butterfly tetranuclear clusters that are related to the *closo*-$Mo_6(\mu_3\text{-}X)_8X_6^{2-}$ structure. The Mulliken population analysis has shown that the bonding in the butterfly clusters is dominated by the influence of the capping ligands whereas the bonding in the square clusters of the same formula is dominated by the edge-bridging ligands. Radial ligands on both the square and butterfly clusters have been shown to be in competition for σ-density between metal–metal cluster bonding and metal–radial ligand bonding, and this phenomenon has been termed the *radial cluster influence*. One manifestation of this is that the metal–radial ligand bond lengths are unusually long as seen in the crystal structures of the characterized clusters: Mo–O terminal and radial distances for O-*i*-Pr ligands in $Mo_4Br_3(O\text{-}i\text{-}Pr)_9$ differ by ca. 0.1 Å.[2] The *radial cluster influence* may have important consequences toward ligand substitution reactions on these clusters and leads us to predict that the radial ligands are likely to be substitutionally more labile: a *radial cluster effect* is anticipated, and this is already known for the substitution chemistry of $Mo_6(\mu_3\text{-}X)_8L_6$ compounds.[42]

There are some rather interesting observations that can be made concerning halide versus alkoxide π-donor ability to the Mo_4 cluster. For each ligand type, the alkoxide ligand has a stronger interaction with the cluster core than the halide ligand. This can be attributed to (i) the energetic difference between O 2p and Cl 3p atomic orbitals relative to the Mo 4d atomic orbitals as seen in the diagonal Fock matrix elements of the converged calculations and (ii) the magnitude of atomic orbital overlap. Although the Mo 4d and Cl 3p energy gap is smaller than the Mo 4d and O 2p gap, the $\langle 4d|3p\rangle$ overlap is small too because of the longer metal–ligand bond and more diffuse valence orbitals. As a consequence, the alkoxide ligand is the better donor to molybdenum

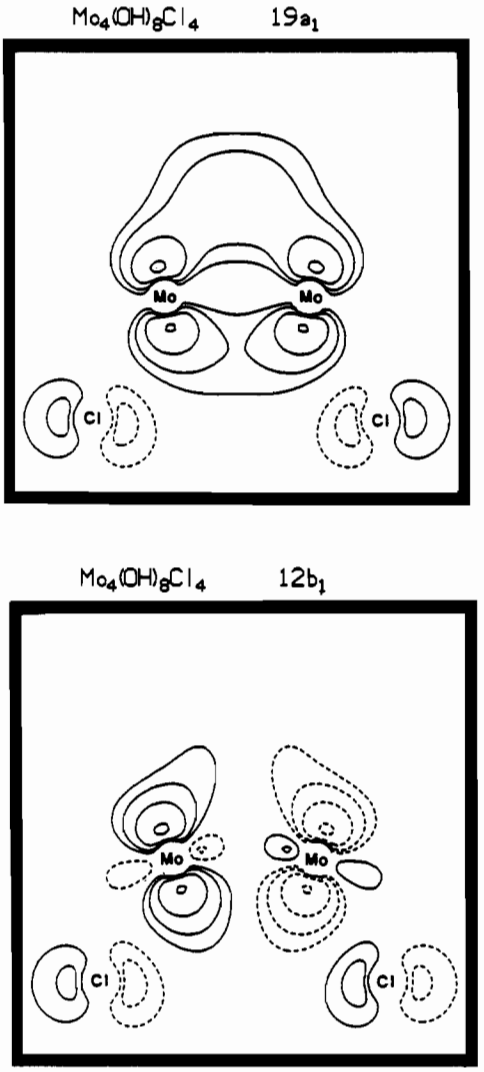

Figure 13. Contour plots of the backbone-localized $19a_1$ HOMO (top) and $12b_1$ LUMO (bottom) of C_{2v} $Mo_4(\mu_3\text{-}OH)_2(\mu_2\text{-}OH)_4(OH)_2Cl_4$. These plots are taken in a plane bisecting the backbone of the Mo_4 butterfly and containing the two backbone Mo atoms and radial Cl ligands.

and preferentially occupies bridging sites over the halide ligand in the mixed halo alkoxy clusters. Moreover, the strong bonding interaction between the O 2p atomic orbitals of the face-capping ligands and the central butterfly core may be largely responsible for the proliferation of alkoxide-supported butterfly clusters.

From these calculations it is shown that the rectangular cluster $Mo_4(\mu_2\text{-}Cl)_8Cl_4^{3-}$, reported by McCarley,[3] is closely related to the square cluster of the same general formula, and the rectangular geometry can be understood as a result of a first-order Jahn–Teller distortion of the regular D_{4h} square structure in analogy with the cyclobutadiene radical cation. Finally, it is interesting to note that the framework-bonding molecular orbitals found for $Mo_4(\mu_3\text{-}X)_2(\mu_2\text{-}X)_4X_6$ butterfly clusters show a distinct similarity to those found by Fehlner and Housecroft,[43] Harris,[44] and Hoffmann[45] in their studies on carbido butterfly clusters. These investigators all found that the butterfly geometry allows for strong interaction between the carbido carbon p orbitals and both the wingtip and backbone iron atoms in $Fe_4C(CO)_{12}^{2-}$. These observations lead us to the prediction that the butterfly clusters $Mo_4(\mu_3\text{-}X)_2(\mu_3\text{-}X)_4X_6$ may be further reactive toward small un-

(42) Chisholm, M. H.; Heppert, J. A.; Huffman, J. C. *Polyhedron* **1984**, *3*, 475.
(43) Fehlner, T. P.; Housecroft, C. E. *Organometallics* **1984**, *3*, 764.
(44) Harris, S.; Bradley, J. S. *Organometallics* **1984**, *3*, 1086.
(45) Wijeyesekera, S. D.; Hoffmann, R.; Wilker, C. N. *Organometallics* **1984**, *3*, 962.

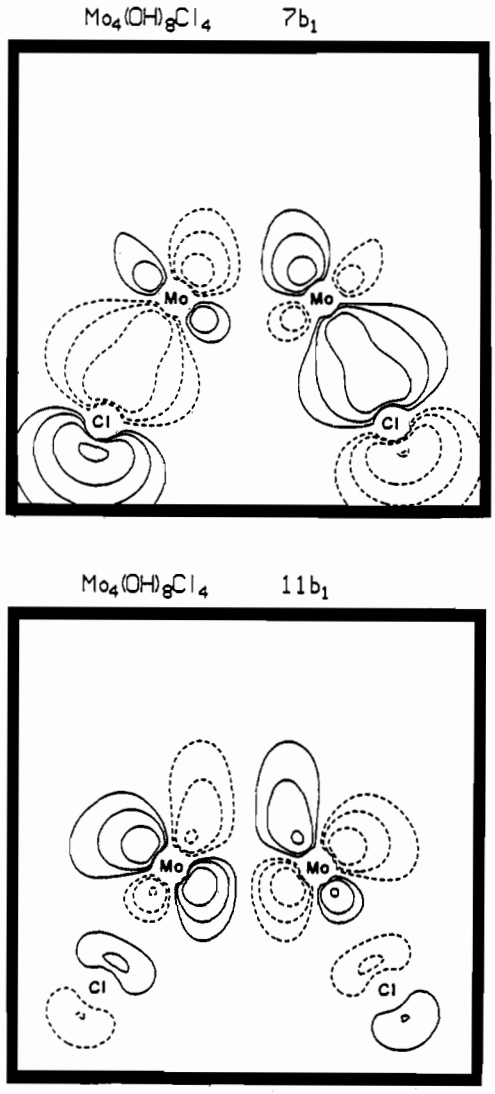

Figure 14. Contour plots of the backbone-localized $7b_1$ (top) and $11b_1$ (bottom) orbitals of C_{2v} $Mo_4(\mu_3\text{-}OH)_2(\mu_2\text{-}OH)_4(OH)_2Cl_4$.

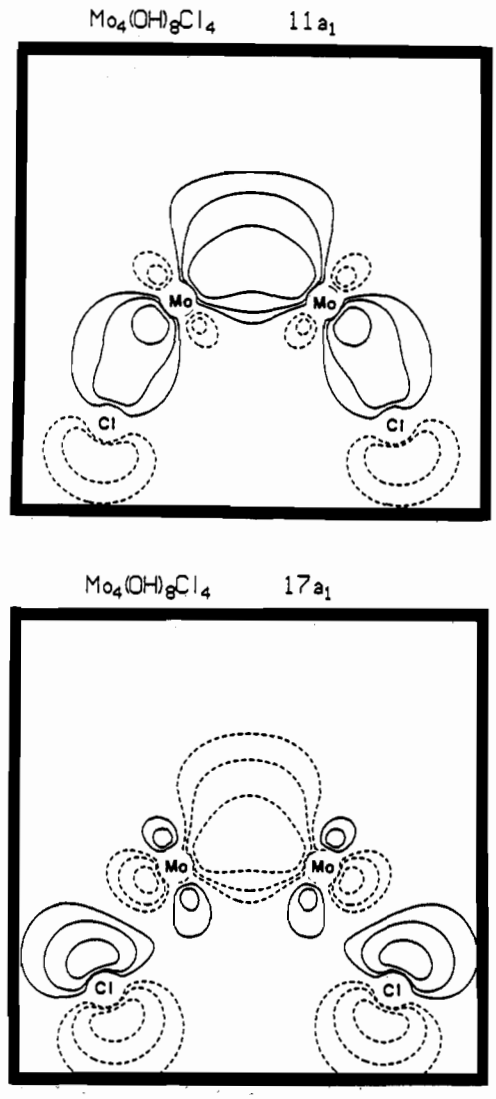

Figure 15. Contour plots of the backbone-localized $11a_1$ (top) and $17a_1$ (bottom) orbitals of C_{2v} $Mo_4(\mu_3\text{-}OH)_2(\mu_2\text{-}OH)_4(OH)_2Cl_4$.

saturated molecules such as carbon monoxide or acetylene.

Calculational Details

Model systems of formula $Mo_4(OH)_8Cl_4$ and Mo_4Cl_{12} were used to investigate the electronic structure and bonding in the square, rectangular, and butterfly geometries. In order to make the calculations tractable, OH has been used as a model for the O-*i*-Pr ligand.

The coordinates for the model square $Mo_4(\mu_2\text{-}OH)_8Cl_4$ cluster were taken from the crystal structure of $Mo_4(\mu_2\text{-}O\text{-}i\text{-}Pr)_8Cl_4$[1] and were idealized to D_{4h} point symmetry. The Mo–Mo distance used was 2.376 Å, and the metal to μ_2-O and terminal Cl distances were 2.026 and 2.440 Å, respectively. The O–H distance was assumed to be 0.960 Å. The same Mo–Mo and terminal Mo–Cl distances were used for the hypothetical $Mo_4(\mu_2\text{-}Cl)_8Cl_4$ D_{4h} square cluster with a metal to μ_2-Cl distance of 2.450 Å. The results of these calculations were transformed into the canonical orbitals of Mo_4^{12+} at the same Mo–Mo distance.

The coordinates for the rectangular $Mo_4(\mu_2\text{-}Cl)_8Cl_4^{3-}$ cluster were idealized to rectangular D_{2h} symmetry by using averaged bond lengths and angles from the crystal structure of $[Ph_4As]_2[Et_4N][Mo_4(\mu_2\text{-}Cl)_8Cl_4]$.[3] The Mo–Mo distances used were 2.655 and 2.353 Å for the long and short rectangular edges, respectively.[46] The Mo to μ_2-Cl and terminal Cl distances were averaged to 2.469 and 2.510 Å, respectively. The results of these calculations were transformed into the canonical orbitals of Mo_4^{10+} at the same Mo–Mo distances.

The coordinates for the model butterfly cluster $Mo_4(\mu_3\text{-}OH)_2(\mu_2\text{-}OH)_4(OH)_2Cl_4$ were taken from the crystal structure of $Mo_4Br_4(O\text{-}i\text{-}Pr)_8$[1] and were idealized to C_{2v} symmetry. The Mo–Mo distance was 2.513 Å for the four edges of the butterfly, 2.493 Å for the backbone Mo–Mo distance, and 3.290 Å from wingtip to wingtip. The metal to μ_3-O, μ_2-O, and terminal O distances were 2.150, 2.030, and 1.840 Å, respectively, and the Mo–Cl distance was assumed to be 2.440 Å as seen for $Mo_4Cl_4(O\text{-}i\text{-}Pr)_8$. The O–H distance was assumed to be 0.960 Å. The same Mo–Mo and terminal Mo–Cl distances were used for the hypothetical $Mo_4(\mu_3\text{-}Cl)_2(\mu_2\text{-}Cl)_4Cl_6$ cluster while the metal to μ_3-Cl and μ_2-Cl distances of 2.500 and 2.440 Å were taken from the crystal structure of $[Et_4N]_3Mo_4Cl_{12}$.[3] The results of these calculations were transformed into the canonical orbitals of C_{2v} Mo_4^{12+} at the same Mo–Mo distances.

Molecular orbital calculations were performed by using the method of Fenske and Hall, which has been described in detail elsewhere.[22] The Fenske–Hall method is an approximate Hartree–Fock–Roothaan SCF–LCAO procedure, and the final results depend only upon the chosen atomic basis set and internuclear distances. All calculations reported here were obtained at the Indiana University Computational Chemistry Center by using a VAX 11/780 computer system or at The Ohio State University by using an IBM 3081-D computer system. Contour plots were generated on a Talaris 800 laser printer with solid lines representing positive density contours and dashed lines representing negative density contours.

All atomic wave functions were generated by a best fit to Herman–Skillman atomic calculations using the method of Bursten, Jensen, and Fenske.[47] Contracted double-ζ representations were used for the Mo 4d AO's, O 2p AO's, and Cl 3p AO's. Basis functions for the Mo atom were derived for a +1 oxidation state with the 5s exponent fixed at 2.0 and

(46) We are grateful to Professor McCarley for kindly providing these structural details prior to publication. These results are now published in preliminary form: see ref 3.

(47) Bursten, B. E.; Jensen, J. R.; Fenske, R. F. *J. Chem. Phys.* **1978**, *68*, 3320.

the 5p exponent fixed at 1.4. An exponent of 1.16 was used for the H 1s atomic orbital.[48]

Acknowledgment. We thank the National Science Foundation for financial support at Indiana University. We are grateful to Professor R. E. McCarley of Iowa State University for kindly providing us with structural details of $Mo_4Cl_{12}^{3-}$ prior to publication and to Dr. M. G. Gatter of The Ohio State University for technical assistance. D.L.C. was the recipient of the 1984-1985 Indiana University SOHIO Fellowship. We also thank the National Science Foundation for departmental supported instruments at Indiana University (VAX 11/780: Grants CHE-83-09446 and CHE-84-05851). B.E.B. gratefully acknowledges support as a Camille and Henry Dreyfus Teacher-Scholar (1984-1989) and as an Alfred P. Sloan Foundation Fellow (1985-1987).

Registry No. $Mo_4Cl_4^{8+}$, 113860-50-7; $Mo_4(\mu\text{-}Cl)_8^{4+}$, 113860-51-8; $Mo_4(\mu\text{-}OH)_8^{4+}$, 113860-52-9; $Mo_4(\mu\text{-}Cl)_8Cl_4$, 101349-43-3; $Mo_4(\mu\text{-}OH)_8Cl_4$, 113860-53-0.

(48) Hehre, W. J.; Stewart, R. F.; Pople, J. A. *J. Chem. Phys.* **1969**, *51*, 2657.

Contribution from the Christopher Ingold Laboratories, University College London, London WC1H 0AJ, Great Britain

Mixed-Valence Nickel(II)/Platinum(IV) Chain Complexes with 1,2-Diaminopropane. Electronic, Infrared, Raman, and Resonance Raman Studies

Robin J. H. Clark,* Vincent B. Croud,† and Rachel J. Wills

Received October 20, 1987

The synthesis and the electronic, infrared, Raman, and resonance Raman spectra of the new mixed-metal complexes $[Ni(pn)_2][Pt(pn)_2X_2][ClO_4]_4$, where X = Cl, Br, or I and pn = 1,2-diaminopropane, are reported. The electronic spectra are characterized by intense broad intervalence bands with maxima at ca. 24 200, 20 400, and 13 150 cm^{-1} for X = Cl, Br, and I, respectively. The infrared spectra are near superpositions of those of the constituent nickel(II) and platinum(IV) complexes. The resonance Raman spectra are dominated by overtone progressions in ν_1, the symmetric $X\text{-}Pt^{IV}\text{-}X$ stretch, reaching $5\nu_1$ for X = Cl or Br and $3\nu_1$ for X = I. Structure was observed in the ν_1 and associated overtone bands for all the complexes; both this structure and the dependence of the band wavenumbers on the excitation line are discussed. The spectroscopic results indicate that the Ni^{II}/Pt^{IV} complexes have weaker metal-center interactions, i.e. more localized valences, than analogous Pt^{II}/Pt^{IV} complexes have. The nature of emission bands occurring in the resonance Raman spectra is also discussed.

Introduction

The relationship between the optical and electrical properties of mixed-valence, linear-chain complexes of platinum and palladium, which are one-dimensional semiconductors, is of considerable interest.[1,2] The vibrational and electronic spectral properties of Pt^{II}/Pt^{IV} [3] and to a lesser extent of Pd^{II}/Pd^{IV} [4,5] and Pd^{II}/Pt^{IV} [6] complexes have been well documented. It has been demonstrated that, for a given metal and halogen, the wavenumber of the symmetric $X\text{-}M^{IV}\text{-}X$ stretching vibration (ν_1) can be correlated with the chain conductivity of the complex. Recently we completed an investigation of mixed-metal complexes of the type $[Ni(en)_2][Pt(en)_2X_2][ClO_4]_4$, where en = 1,2-diaminoethane and X = Cl, Br, or I,[7] and demonstrated that the degree of metal-center interaction was intermediate between that of analogous Pt^{II}/Pt^{IV} and Pd^{II}/Pt^{IV} complexes. In order to study further the effect of substituting Pt^{II} by Ni^{II}, we have extended our studies to Ni^{II}/Pt^{IV} complexes containing 1,2-diaminopropane as the off-axial ligand and Cl, Br, or I as the bridging group.

Experimental Section

(a) Preparations. The mixed-valence complexes were prepared by mixing the appropriate aqueous solutions of $[Ni(pn)_2]^{2+}$, $[Pt^{IV}(pn)_2X_2]^{2+}$, and $Na[ClO_4]$. The ions $[Pt^{IV}(pn)_2X_2]^{2+}$ were made by dihalogen oxidation of $[Pt^{II}(pn)_2]^{2+}$ except for the iodide, which was made by addition of KI to an aqueous solution of $[Pt^{IV}(pn)_2Br_2]^{2+}$. All platinum(IV) species were checked for complete oxidation by adding an excess of $Na[ClO_4]$ to an aqueous solution of the platinum(IV) species and looking for any color changes characteristic of the formation of the complexes $[Pt(pn)_2][Pt(pn)_2X_2][ClO_4]_4$. The iodide complex was difficult to obtain, probably due to rapid displacement of the amine from $[Ni(pn)_2]^{2+}$ by iodide.

Repeated attempts to recrystallize the Ni^{II}/Pt^{IV} complexes led to a gradual reduction of the Pt^{IV} moiety to Pt^{II} and then to contamination of the product with the analogous Pt^{II}/Pt^{IV} chain complex. As a consequence only fairly small crystals were grown, which did not prove suitable for single-crystal Raman work. Anal. Calcd for $[Ni(pn)_2][Pt(pn)_2Cl_2][ClO_4]_4$: C, 14.14; H, 3.96; Cl, 20.87; N, 11.00. Found: C, 14.2; H, 3.96; Cl, 20.6; N, 10.95. Calcd for $[Ni(pn)_2][Pt(pn)_2Br_2][ClO_4]_4$: C, 13.01; H, 3.64; total halogen as Cl, 19.20; N, 10.11. Found: C, 13.0; H, 3.50; total halogen as Cl, 19.4; N, 10.14. Calcd for $[Ni(pn)_2][Pt(pn)_2I_2][ClO_4]_4$: C, 11.99; H, 3.35; N, 9.32; I, 21.11. Found: C, 11.7; H, 3.30; N, 9.35; I, 20.5%.

(b) Instrumentation. Electronic spectra were recorded on a Varian 2390 spectrometer as Nujol mulls of the samples, between quartz plates, at room temperature.

Infrared spectra were recorded in the region 650-20 cm^{-1} on wax disks of the complexes, by using a Bruker IFS 113 V interferometer. The spectra were obtained at ca. 80 K by using an RIIC cryostat cooled by liquid nitrogen.

Raman spectra were recorded on a Spex 14018/R6 spectrometer. Exciting radiation was provided by Coherent Radiation Model CR 12 and CR 3000 K lasers, the powers being kept to <50 mW. Samples for Raman spectra were in the form of pressed disks of the pure complexes and were held at ca. 80 K with use of a liquid nitrogen and Dewar assembly and at lower temperatures by using an Air Products Displex cryostat. Spectra were calibrated by reference to the Rayleigh line.

Results and Discussion

Electronic Spectra. Crystals of the complexes are dichroic. The chloride is yellow with the electric vector of the incident beam parallel to the chain (z) axis and colorless when the vector is perpendicular to it. The bromide is likewise blue and orange, respectively, and the iodide is dark blue and red, respectively. The bromide and iodide have a strong metallic sheen, which is lost on their being ground to powders. The colors of the crystals and powders together with related spectroscopic data are given in Table I.

† Present address: Borax Research Ltd., Cox Lane, Chessington, Surrey KT9 1SJ, Great Britain.

(1) Brown, D. B., Ed. *Mixed-Valence Compounds*; D. Reidel: Dordrecht, The Netherlands, 1982.
(2) Miller, J. S., Ed. *Extended Linear-Chain Compounds*; Plenum: New York, 1982; Vol. 1-3.
(3) Clark, R. J. H. *Adv. Infrared Raman Spectrosc.* **1985**, *11*, 95.
(4) Clark, R. J. H.; Croud, V. B.; Kurmoo, M. *Inorg. Chem.* **1984**, *23*, 2499.
(5) Clark, R. J. H.; Croud, V. B.; Kurmoo, M. *J. Chem. Soc., Dalton Trans.* **1985**, 815.
(6) Clark, R. J. H.; Croud, V. B. *Inorg. Chem.* **1985**, *24*, 588.
(7) Clark, R. J. H.; Croud, V. B. *Inorg. Chem.* **1986**, *25*, 1751.

0020-1669/88/1327-2096$01.50/0